Effects of Vegetation-Sediment Interactions on the Morphological Evolution of Coarse-Bedded Rivers: Results from Flume Experiments

A Thesis
SUBMITTED TO THE FACULTY OF
UNIVERSITY OF MINNESOTA
BY

Virginia Alderson Batts

IN PARTIAL FULFILLMENT OF THE REQUIREMENTS
FOR THE DEGREE OF
MASTER OF SCIENCE

Karen B. Gran

July 2017

Acknowledgements

I am infinitely grateful for all of the students, faculty, and staff for their help in this study. First and foremost, I would like to thank my advisor, Dr. Karen Gran, for her wisdom, inspiration, and support, but especially her patience. I would also like to thank my committee members, Drs. John Swenson and Chris Lenhart, for their attention and also their guidance throughout those two years.

This project would not have been possible without the carpentry expertise of Martin Bevis and the technical know-how of Edward Gazzetti, both of whom played critical roles in flume construction. To both of you, I extend my deepest gratitude. Design and construction for flume accessories were provided by Mike Plante and Mark Roberts in the Department of Civil and Environmental Engineering at UMD – thank you!

I am also profoundly grateful for the undergraduate students who dedicated their time to helping me. Robbie Eisenrich, thanks a lot for your patience and cheerful assistance while I was developing my methodology. To Amber Michels – your dedication and enthusiasm are gold. Thank you for your help with data processing and analysis.

Funding for this research was provided by the National Science Foundation (EAR-1209402). Access and use of the terrestrial lidar scanner was made possible by the University of Minnesota's Office of the Vice President for Research through the I^3 Initiative. Funding to present this research was provided by travel grants from the Swenson College of Science and Engineering, the Department of Earth and Environmental Sciences, and the Water Resources Science program at the University of Minnesota, Duluth.

Dedication

This thesis is dedicated to my loving family, whose unending support has made all of this possible.

Abstract

Laboratory experiments over the past two decades have demonstrated the crucial role of vegetation in determining the morphological characteristics of river channels. Through a series of flume experiments, this research builds on previous studies by examining the respective role of both vegetation and sediment load composition on resulting channel planform style and dynamics as vegetation density increases. I used a 1.5 m by 6 m flume filled with well-sorted quartz sand (D_{50} = 0.5 mm) to simulate a gravel-bedded river. Each experiment simulated a series of 4-hour floods, after each of which the flume was seeded with alfalfa (*Medicago sativa*) so that vegetation density increased with each flood. The only variable between the two experiments was the composition of the sediment feed. We fed only bed load in Experiment 1, and both bed load and suspended load in Experiment 2.

Confirming the findings of earlier experiments, vegetation progressively stabilized the surface of the flume, limiting the number of channel threads until only one remained. The resulting channel was deeper, faster, and narrower than the unvegetated channel. Results suggest that vegetation-sediment interactions can produce widely differing channel morphology depending on the composition of sediment load and the frequency of overbank flows. They also demonstrate that while bedload transport within a channel with strengthened banks is critical for the generation of a meandering pattern by building bars, fine sediment may play an equally important role in adjusting floodplain topography. The amount, distribution, and storage of sediment trapped in the riparian corridor were directly related to vegetation density and the presence of overbank flows.

Table of Contents

List of Tables

List of Figures

Introduction

Natural rivers exhibit a wide range of planform patterns, such as braided, sinuous, meandering, or straight. Particular channel patterns arise from variability in climatic and geologic settings, which set a number of important factors: slope, bank strength, sediment load, hydrologic regime, and roughness. These factors determine lateral and vertical mobility, sediment transport capacity, and the frequency of channel-floodplain interactions, thereby driving channel morphodynamics. As climate and geology vary widely across the globe, so do river channel patterns. However, the complexity involved in studying river channels goes beyond geographic variability. When it comes to individual channel morphodynamics, none of these factors exist in isolation. Rather, all are connected through biologic, hydrologic, and geomorphic feedback processes. Individual processes that contribute to channel form are often difficult to observe and quantify in situ, however, because they occur over wide ranges of spatial and temporal scales.

One feedback process related to most rivers on earth relates flood regime with the creation and destruction of riparian vegetation, and the transport and storage of sediment (Corenblit et al, 2007; Murray et al, 2008; Gurnell, 2013; van Dijk, 2013). During high-magnitude floods, riparian vegetation is destroyed by bank erosion. As these floods recede, mobilized seeds and other propagules are deposited on exposed surfaces: a process known as hydrochory (Nilsson et al, 1991). This allows vegetation to colonize fluvial landforms (Gurnell et al., 2004). Field observations and experimental studies have

shown that vegetation plays a primary role in controlling alluvial channel morphology by increasing surface cohesion (Millar, 2000; Hession et al, 2003; Brooks et al, 2003). By strengthening near-channel surfaces, vegetation consolidates flow into fewer channel threads, thereby lowering width/depth ratios and increasing channel velocity (Gran and Paola, 2001). Because this effect strengthens with vegetation density, vegetation density plays a large role in determining where along the channel pattern continuum (Leopold and Wolman, 1957) a particular river lies. At one end, unvegetated channels migrate freely and rapidly across an unconsolidated floodplain, continually widening until braiding occurs and channel bars form. At the other end are single-thread meandering channels in a densely-vegetated floodplain where channel width is limited by bank strength, so channel banks erode at rates that compare with the growth of inner bars.

Laboratory experiments (Gran and Paola, 2001, Tal et al, 2004; Tal and Paola, 2007, Tal and Paola, 2010) have shown that simply through the repeated addition of vegetation, unvegetated braided channels will reorganize themselves into single thread channels that exhibit some meandering behavior - making a complete shift from one end of the continuum to the other. However, these experiments did not focus on the interactions of vegetation and sediment load, which is a critical third component of biogeomorphic feedback processes in rivers. When vegetation interacts with flood flows, stems and leaves add turbulence and hydraulic drag, acting to slow channel velocity and causing sediment to fall out of suspension. By inducing sediment deposition and preventing further erosion, vegetation can 1) trap and store sediment on channel bars and in the floodplain, which on larger scales may impact a river's sediment budget, and 2)

contribute to the growth and development of fluvial landforms, which progresses the evolution of river channel pattern. Unfortunately, the episodic and spatially-complex nature of this process makes it extremely difficult to observe in the field. In the lab, vegetation-induced deposition has been well-studied at the plant or patch scale (Nepf, 1999; Tabbacci et al. 2000; James, et al, 2004; Chen et al, 2011; Liu et al, 2010; Nepf, 2012; Luhar and Nepf, 2013). There is more to learn about vegetation-sediment interactions at a scale that would reveal their overall impact on channel morphology.

How does vegetation influence the storage and transport of sediment - not only at each morphologic end member but as a channel network reorganizes from one to the other? Can the presence or absence of a fine-sediment fraction have an equally-important role in resulting channel morphology to vegetation establishment? Answers to these questions are important for two reasons. Scientifically, it is important to understand how changes in floodplain composition (i.e. vegetation and surface substrate) result in different fluvial landforms and channel patterns. Perhaps even more important, from a management perspective, is to know how channel change affects a river's ability to store and/or transport sediment, as in some cases suspended sediment is considered a pollutant.

In order to address these questions, I conducted flume experiments to observe the way a braided river's sediment load interacts with encroaching vegetation, and how this interaction impacts channel morphodynamics. These experiments simulate a self-formed, gravel-bed braided channel that is increasingly colonized with young riparian trees – similar to willows or cottonwoods. I imposed a two-stage hydrograph, where maximum discharge was held for a four-hour period. Discharge was then halved for approximately

15 minutes while the flume was seeded with alfalfa (*Medicago sativa*) at a specified density. This was intended to simulate the deposition of seeds on exposed surfaces by wind or receding flood flows. Discharge was then reduced to subsurface flow in order to keep the surface moist over a six-day period while seeds germinated and sprouted. This process was repeated over the course of seven weeks for Experiment 1, and ten weeks for Experiment 2, so that seed density and floodplain cohesion increased after every four-hour flood. The only variable that changed between the two experiments, other than total experiment length, was the composition of the sediment feed. In Experiment 1, only sand (simulating bed load) was fed into the system during floods. In Experiment 2, I fed a 1:1 mixture (by volume) of sand and a synthetic plastic sediment - representing a suspended fraction - at the same rate as Experiment 1.

In agreement with similar studies, our experiments showed that vegetation is a primary control on channel flow dynamics and geometry. Here, however, varying the composition of the sediment feed resulted in two channels with very different flow dynamics and geometry. With a higher feed of sand and without a fine sediment fraction, the channel in Experiment 1 was unable to generate meander bends due to rapid channel aggradation and continual constriction of the floodplain by vegetation. By lowering amount of sand and introducing a suspended fraction to the sediment feed in Experiment 2, I was able to generate a sustained meandering channel, where vegetation-induced deposition of fine sediment within the floodplain contributed to floodplain construction. These differences became evident during conditions of overbank flow, which suggests that they were driven by vegetation-sediment interactions.

Literature Review

In the past three decades, there has been a growing body of research focused on better understanding the reciprocal relationships between riparian vegetation and fluvial morphodynamics. This interdisciplinary field, termed "biogeomorphology" (Phillips, 1995; Naylor et al., 2002; Stallins, 2006; Corenblit et al., 2007; Murray et al., 2008), connects ecology with geomorphology in the study of biotic-abiotic feedback relationships that control surficial processes. In the study of fluvial systems, the primary goals of biogeomorphology are to describe the role of living organisms in the evolution of fluvial landforms, and the balancing role of hydrogeomorphic processes (i.e. sediment erosion, transport, deposition, and flood regime) in the community structure of riparian ecosystems.

Riparian vegetation, fine sediment, and high-magnitude floods contribute to a biogeomorphic feedback process that drives channel morphology. The root systems of vegetation add tensile strength to soils and sediment (Operstein and Frydman, 2000). Stems and leaves add hydraulic drag (Luhar and Nepf, 2013) and surface roughness (O'Hare et al., 2010), which increases turbulence and decelerates flow, encouraging sediment to fall out of suspension. This process contributes to floodplain construction and enhances bank strength, which controls channel geometry by limiting bank erosion (Beeson and Doyle, 1995; Millar, 2000) and channel widening (Erskine et al., 2012). Floods supply the force for eroding, transporting, and depositing sediment, which drive channel change. Floods are also responsible for the dispersal and burial of seeds, and both

the creation and destruction of vegetation habitats (Sigafoos, 1961). A river's flood regime, or the timing and magnitude of flood events, is therefore an important common denominator between the erosion, transport, and deposition of sediment and the colonization, growth, and reproduction of riparian vegetation (Corenblit et al., 2007). Channel pattern is the net result of this biogeomorphic feedback. Channel pattern is a reflection of bank stability, flood frequency, and sediment dynamics, all of which affect or are affected by the colonization and growth of riparian vegetation. However, these processes occur on temporal and spatial scales that are often difficult to observe in situ. Understanding how changes in sediment load, flood frequency, or vegetation density may affect channel morphodynamics may be best captured in the laboratory.

Physical Modeling of Fluvial Systems: Previous Experiments

There has been a growing interest in examining the roles of vegetation, flow regime, and sediment transport on channel pattern in a controlled setting (Gurnell, 2013). Unlike field-based approaches, laboratory approaches offer the ability to speed up time and shrink space to study natural processes that cannot be observed in situ. Experiments also provide the ability by isolate certain variables by keeping others constant, thereby simplifying a complex system to observe distinct elements. Experimental flumes have been highly valuable in this regard, because they are technologically simple yet highly effective in modeling landscape-scale processes. Further, laboratory-scale application of remote sensing technologies has enhanced measurement capabilities of velocity (Doppler velocimetry, as in Nepf (1999)), depth and diffusivity (image-based dye density

techniques, as in Gran and Paola (2001), Tal et al. (2004)) and planform change (small-scale lidar applications, as in van Dijk et al. (2012)) in physical models.

This study builds upon the methods of previous experimental studies of the reciprocal relationships between channel flow, sediment transport, and riparian vegetation. These studies (Gran and Paola, 2001; Tal and Paola, 2007, Braudrick et al., 2009, van Dijk et al., 2012) used alfalfa *(Medicago sativa*) to represent riparian vegetation. Pollen and Simon (2006) determined that after a growth period of 7-21 days, alfalfa sprouts geometrically represent young riparian trees, such as willow or cottonwood. Further, measurements of cohesion provided by root strength at a range of stem densities were comparable to other studies relating root strength to braiding intensity.

Gran and Paola (2001) were the first to develop an experimental method using alfalfa in a flume (Figure 1) to investigate the role of riparian vegetation on gravel-bed channel form and flow. They compared self-formed, braided river networks with and without alfalfa, varying only the spatial density of stems in between runs. Each experiment involved the generation of a braided network at a constant discharge followed by the seeding of the bed while at half of the normal discharge rate. After a growth period of 10-20 days, normal discharge rate was resumed. In both the non-vegetated and vegetated braided systems, channel depth, channel velocity, and bed elevations were measured in order to compare the two systems. Gran and Paola found that as vegetation density increases, channel braiding intensity, width to depth ratio, and lateral mobility decrease, while channel velocity, maximum depth, and relief increase. These experiments

demonstrated that by stabilizing channel banks and limiting channel migration, vegetation plays an important role in reorganizing braided channels into multi-threaded channels.

However, the results of the study did not address the question of whether vegetation alone can invoke a single-threaded, meandering network from a braided one. Tal and Paola (2007) expanded this methodology to show that indeed, a self-formed braided channel will re-organize into a single threaded channel with the *repeated* addition of vegetation. Experimental runs alternated between periods of high and low flow, and the flume was re-seeded after each high-flow period. Seedlings established on bars exposed during low flow, and acted to slow bank erosion and lateral migration, "corralling" flow into fewer channels. It was the combination of alternate flood regimes and sequential seeding that encouraged the braided channel to reorganize. In braided channel networks, unconstrained flow causes channels to constantly readjust and shift laterally. Tal and Paola showed that instead, channels constrained by vegetation tend to avulse back and forth between fewer available channels. Channels unoccupied at low flow would be choked with vegetation in the following seeding. In this manner, repeated seed dispersals following periods of channel-forming flows reduced a braided channel to a dynamic single-thread channel that exhibited behavior fluctuating between "wandering and irregularly sinuous". At steady state, they observed bank erosion as well as point-bar development, which led to the expansion of channel bends and active meandering (Figure 2) with chute cutoffs.

Braudrick et al. (2009) later conducted similar experiments that demonstrated both vegetation and suspended sediment deposited by periodic overbank flows were necessary to prevent chute cutoffs and maintain a systematically-meandering channel. Rather than starting with a self-formed channel network, these experiments initiated meandering by carving an initial bend in a straight channel. Vegetation was added to the flume in order to increase bank strength and slow outer bend migration. In addition to sand (bedload), non-cohesive lightweight plastic sediment was included in the feed in order to simulate suspended load. Braudrick et al. observed that the plastic sediment filled in chute channels that began to form next to bars, preventing channel cutoffs and therefore encouraging sustained, systematic meandering.

Later, van Dijk et al. (2012) achieved a self-sustained, dynamic meandering channel in the lab without vegetation. The experiments demonstrated that the inclusion of fine silt in the sediment feed combined with a flood regime that included overbank flows, sustained meandering by continually rebuilding floodplain and preventing chute cutoffs. Experimental channels without fine sediment tended to braid and lose sinuosity, while channels with fines sustained lateral migration and increased in sinuosity over the course of the experiment (Figure 3). The floodplain of the meandering river was formed and re-formed by two mechanisms a) the deposition of sand and silt on inner banks, resulting from lateral migration and b) the overbank enrichment of silt on outer banks, by vertical accretion. Fine sediment deposition also stabilized channel banks while decreasing bank erosion, which prevented local avulsions and chute cutoffs.

Research Objective

Results from recent experiments point towards bank stability and overbank deposition as two necessary elements in the development of a single-thread meandering channel. Vegetation provides bank strength, while fine sediment fills chute cutoffs and prevents their reoccupation. However, there is more to be gained from experiments combining vegetation and fine sediment. For example, what are the respective roles of vegetation encroachment and fine sediment deposition in driving channel transition from one pattern to another? How do these two factors interact as a channel network reorganizes? Answers to these questions are not only important scientifically but are also highly applicable to river management. Anthropogenic changes of floodplain composition and flood regime, either through land development or climate change, have been shown to affect channel morphology and behavior. In the short term, these changes can have negative effects on riparian habitats, which are highly adapted to local flood regime and sediment dynamics. Understanding the respective roles of vegetation and sediment dynamics on channel morphology will improve our ability to predict the effects of environmental change on river corridors.

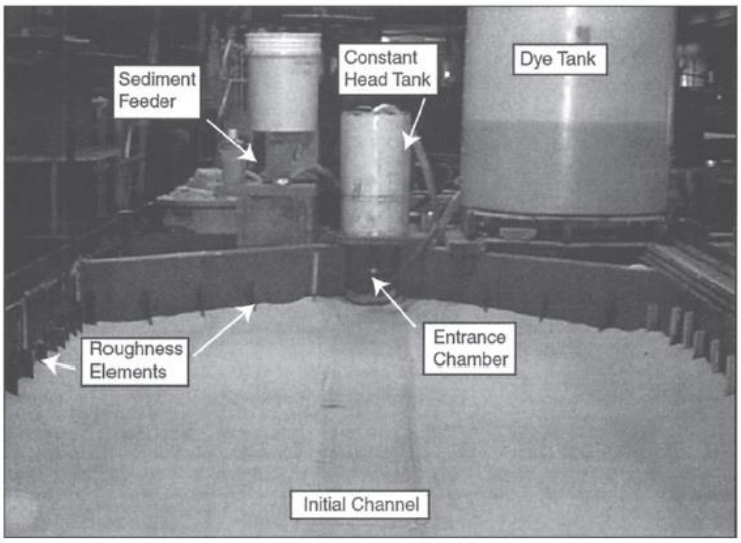

Figure 1. Experimental set-up used by Gran and Paola (2001).

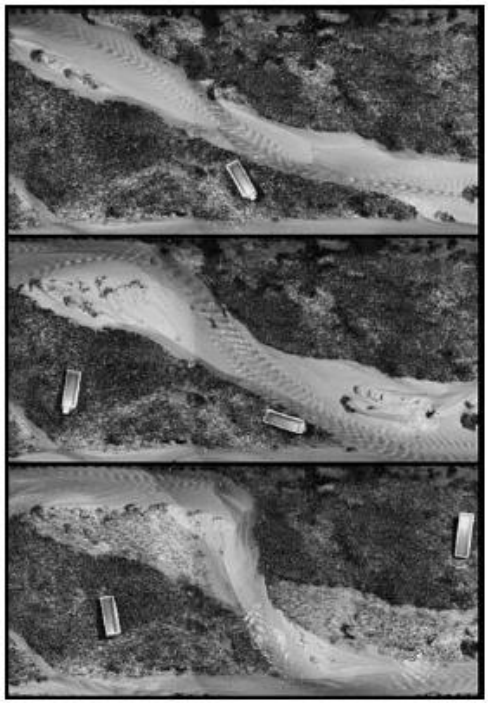

Figure 2. Bar development from Tal et al. (2010).

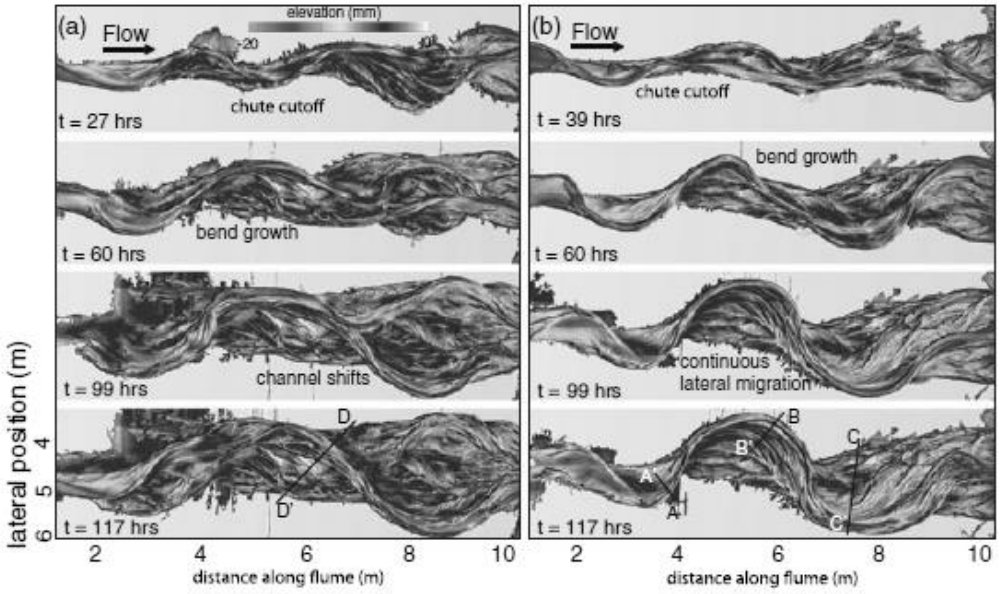

Figure 3. Channel evolution shown in DEMs of van Dijk et al. (2013).

Methods

Experimental Set-up

I built a 1.5 m x 6 m flume for these experiments at the Large Lakes Observatory at the University of Minnesota, Duluth. The bed was built to a slope of 0.01 and filled with dry quartz sand (D_{50} = 0.5 mm), which was graded to achieve an initial bed slope of 0.015. Each experiment began with a flat, graded bed with an initial channel carved down the middle, approximately 1.5 cm deep by 15 cm wide, to initiate channel flow. Each experiment maintained a constant discharge (Q_W) of 3.0 x10^{-4} m^3/s at low flow (only during seeding, approximately 15 min) and 6.0 x10^{-4} m^3/s at flood flow. Discharge was recirculated from a 378 L tank at the end of the flume and delivered from a constant-head tank at the headwall. Inflow from the constant head tank was aimed at the headwall to reduce turbulence and scouring at the entrance (Figure 4.A). A rectangular weir was

installed at the end of the flume, the base of which was built to the height of the sand bed to reduce backwater effects (Figure 4.B). To avoid other possible entrance and exit effects, I collected depth, velocity, and bed elevation data only between 2.0 and 4.0 m downstream of the headwall, at cross-sectional transects set 0.5 m apart – a total of 5 transects named with letters A-E (Figure 5).

Previous experiments using similar approaches found that channels tend to migrate outwards and "stick" to the lateral walls. To prevent this, I shaped a 10-cm wide "terrace" of 0.5 mm sand along the walls (Figure 6). During the unvegetated floods, I re-built the terraces when the channel eroded them in order to avoid starting the experiments with wall effects. When vegetation was added, I seeded the terraces as well to add some strength and roughness, providing a more effective buffer.

Initial slope, water discharge, and sediment feed rate were held constant between both experiments. The only variable that was changed was the composition of the sediment feed. In Experiment 1, I dispensed only 0.5 mm sand through a gravity-driven sediment feeder at a rate of 1.3 g/s. This sand behaved as bed load, and using the Shields curve I estimated that it was mobile at depths above 2 mm (Appendix 1). In Experiment 2, I used a mixture of sand and fine plastic sediment ("Clear-Cut", D_{50} = 0.15 mm, SG = 1.25) at a ratio of three-parts sand to one-part plastic sediment by weight, an approximate 1:1 ratio by volume. This mixture was also fed at 1.3 g/s. Calculating the Rouse number (Appendix 2) for the plastic sediment over a range of expected channel depths in these experiments, I determined that the fine plastic sediment would behave as both bed load and suspended load.

Similarity with Natural Systems

Laboratory-scale models of channel networks exhibit spatial patterns and processes that compare well with natural systems, despite differences in materials or spatial and temporal scales. This has been referred to as the "unreasonable effectiveness" of geomorphic experiments (Paola et al., 2009). Rather than replicating a particular river, these experiments are designed only to model natural river processes to observe trends over time. I tried to maintain similar flow conditions to those of natural rivers and used parameters (discharge, sediment feed, bed slope) similar to those of previous flume experiments of similar scale. To compare similarity of flow conditions between our experiments and natural rivers, I calculated the Froude number (Fr) and Reynolds number (Re) where $Fr = u/\sqrt{gh}$, with u = mean velocity, g = gravity, and h = mean flow depth and $Re = uh/\nu$ where ν = kinematic viscosity. The average Froude number was 1.31 for Experiment 1 and 1.41 for Experiment 2. The average Reynolds Number was 1868 in Experiment 1 and 2260 for Experiment 2. This results in super-critical, turbulent flow conditions. Flow in natural rivers is generally sub-critical, with super-critical flow conditions over short distances or durations. However, super-critical flow conditions are not atypical in large braided rivers with very high sediment loads. Given that similar experiments have maintained sub-critical, turbulent flow conditions using similar parameters, it is possible that our velocity measurements are erroneously high or I have underestimated average depths. More importantly, these experiments demonstrated trends, landforms and other geomorphic features that one might expect to observe in natural systems.

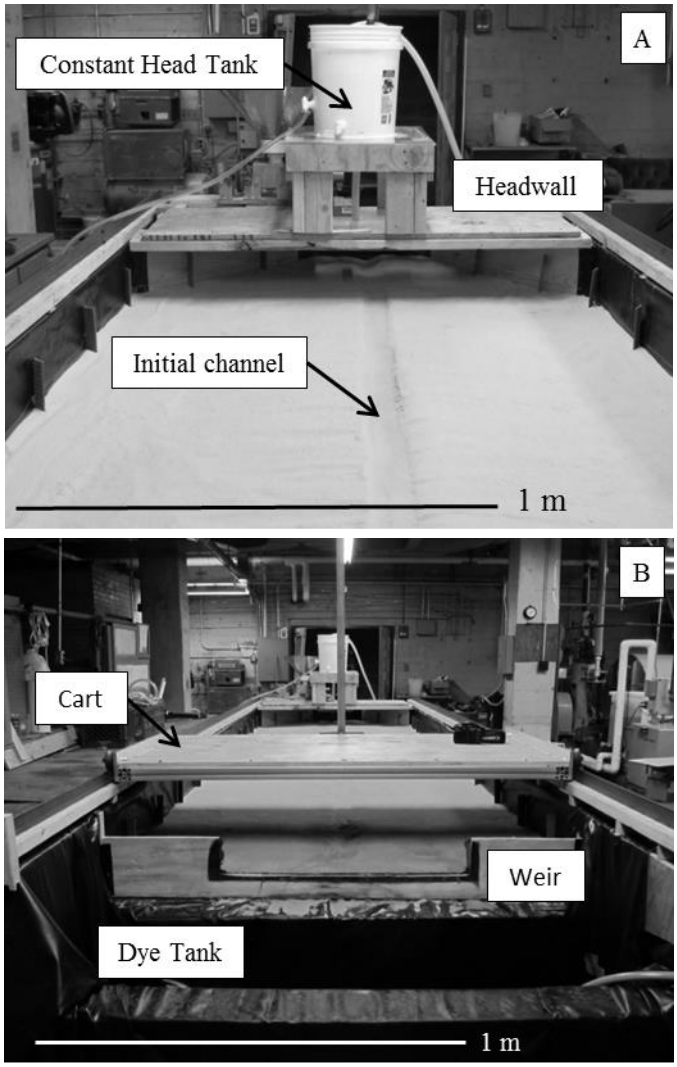

Figure 4. Upstream (A) and downstream (B) views of the experimental set-up.

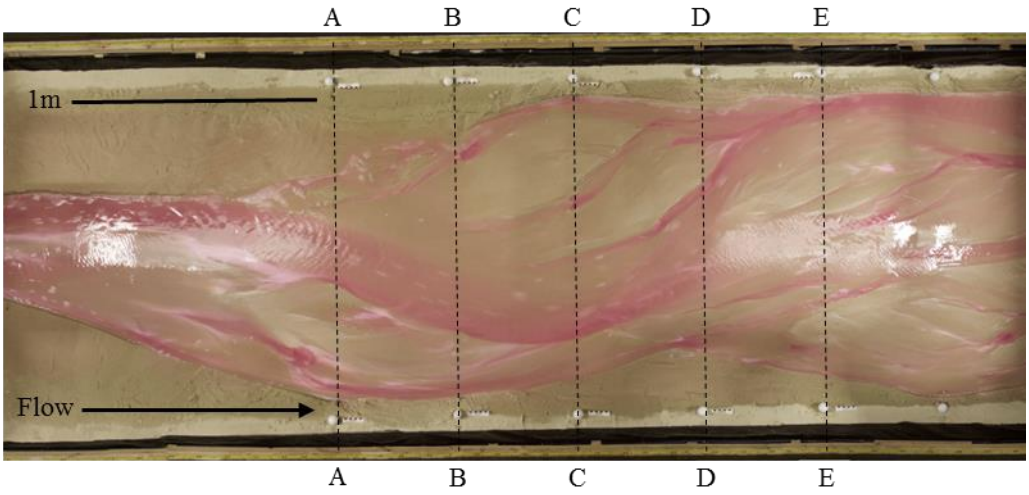

Figure 5. Cross sectional transects used for data collection.

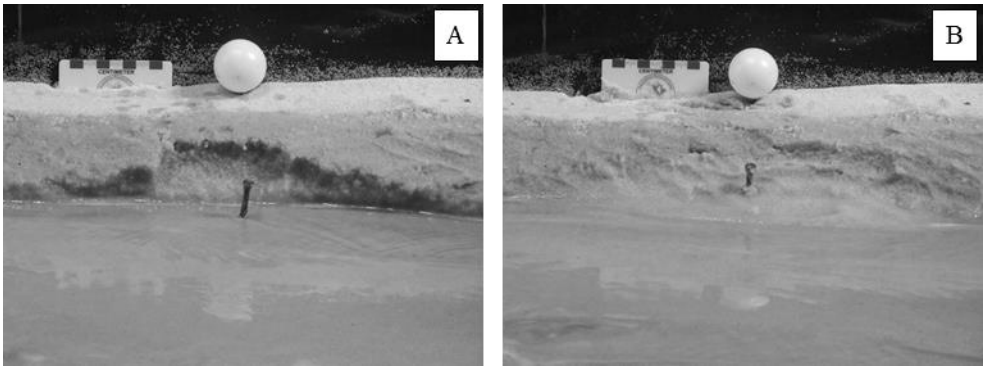

Figure 6. Buffer terraces collapsed (A) and re-built (B).

Vegetation

I modeled vegetation in these experiments using alfalfa (*Medicago sativa*), which I seeded after the flow had incorporated the entire flume surface as a braided network. Water discharge was lowered by 50% during seed dispersal in order to expose channel bars and keep main channels open. Sediment feed was paused during seed dispersal. I determined the appropriate mass of seeds to distribute by multiplying the flume area in cm^2 by the average weight of a single seed and the desired density. During seed dispersal, seeds that landed in occupied channels washed downstream, while seeds that

landed in smaller, low-flow channels and on exposed bars remained. After dispersal, discharge was lowered further to subsurface flow only in order to retain necessary moisture to promote seed germination and growth without disturbing the channels. At later stages in the experiments when channels were deeper, pools held some water during this period. Two fluorescent grow lights were suspended over the flume after a 2-day germination period without light, then turned on for four days – a total of six days for germination and growth between floods. During this period, the sprouts reached a stem height of approximately 30 mm and a diameter of 1 mm. During this period, the sprouts produced a single taproot that was approximately equal to the stem in length, thinning with depth.

Image-Based Techniques for Tracking Flow Conditions

Much of the data from these experiments came from photographic imagery collected by two cameras (Figure 7). I mounted a Canon Powershot (Camera 1) on the ceiling directly above the analyzed portion of the flume to record time-lapse footage at 1 minute intervals. From these photos, I extracted channel depth using a remote dye intensity tracking technique, discussed later. A second camera, a Canon EOS Rebel T3i (Camera 2), was mounted to an aluminum frame that had been fitted to a cart that slides over the flume surface. This camera recorded video footage for channel velocity measurements and also overhead photographs that could be stitched together at a higher resolution than the overhead camera for capturing the full flume length. In addition to capturing surface features at higher resolution, composite images were superimposed on laser scans for referencing when collecting elevation data.

Both cameras were shooting in raw image format in order to retain maximum image quality. I used the Program ("P") shooting option in both cameras, which automatically adjusted aperture and shutter speed while allowing for the manual setting of all other parameters such as white balance and color balance. I set an ISO value of 800 and selected a white balance setting for the ambient, fluorescent light conditions in the room – these manual settings were identical in both cameras. Photographs were converted to an uncompressed (lossless) TIFF file format for adaptability among multiple software programs. Photographs from the camera on the ceiling were uniformly corrected for lens distortion (barrel distortion) in Adobe Photoshop CS4 prior to analysis.

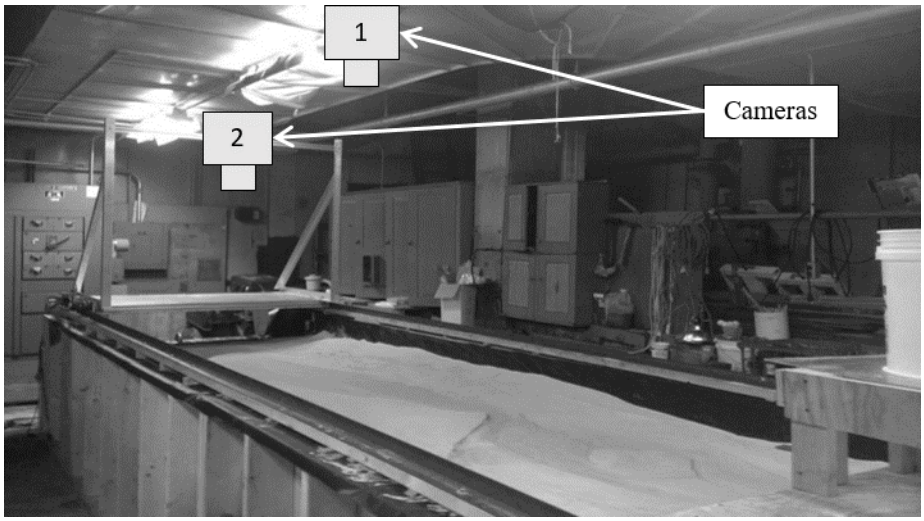

Figure 7. Cameras used in the experiments.

Channel Depth

I tracked changes in channel depth across the flume using a dye-density technique applied by Gran and Paola (2001) and Tal and Paola (2007) to their flume experiments. I circulated 378 L (100 gallons) of 2 ppm Rhodamine WT dye through the flume during floods. Because the intensity of light in the dye color's green band decreases with depth, I

was able to track depth using overhead photographs of the dyed channels. I generated a calibration curve by placing tilted trays at three inactive locations in the flume that had slightly different lighting because they were either directly beneath ceiling lights or in between them (Areas 1, 2, and 3, Figure 8). The calibration trays were coated with sand to match the color of the flume bed, then filled with dyed water from the holding tank to a maximum depth of 4 cm. Because depth increases linearly in the trays, overhead images of the filled trays provided a curve reflecting the relationship between depth and light intensity (Figure 9). I collected calibration curves from all three designated areas every hour to generate a flood-representative curve (Figure 10), which I used to convert green wavelength intensity values to depth. I used the same images to extract cross-sectional color profiles of the channels every two hours on all five transects. Occasionally, color profiles of the channels had reflections in them. These were manually extracted from the data.

To verify our calibration, I manually measured depths at 30 locations throughout each experiment using a point gauge. All measurements were taken along the delineated transects. Care was taken to ensure equal coverage of measurements over all transects. The average difference between the manually-measured depth and the depth measured from the images was 1.8 mm for Experiment 1 and 1.2 mm for Experiment 2.

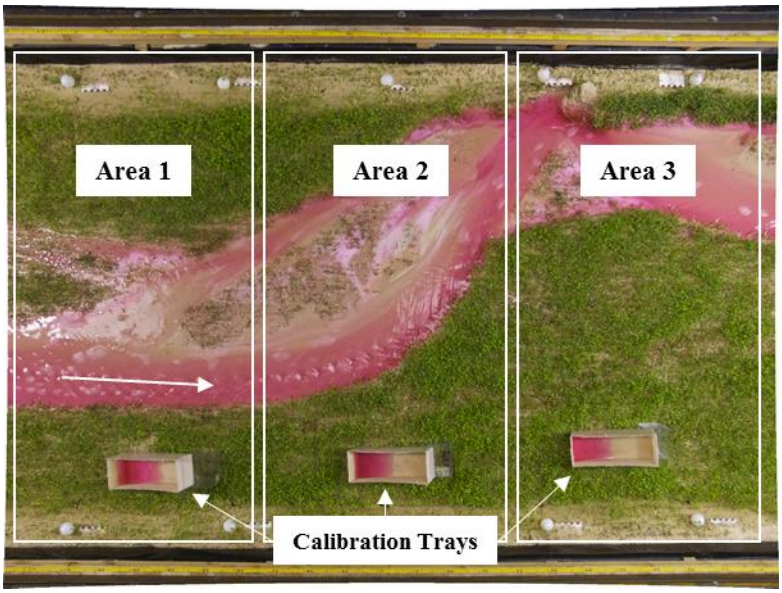

Figure 8. Areas of common lighting for depth calibration.

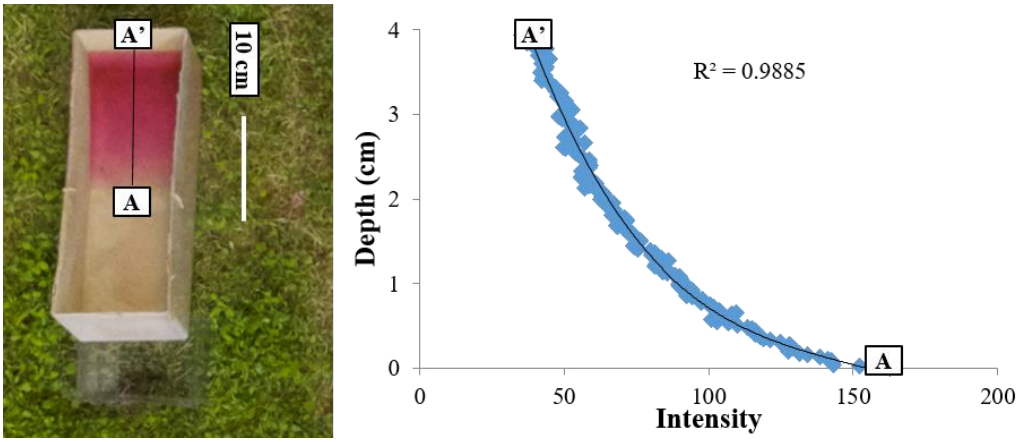

Figure 9. Depth calibration example.

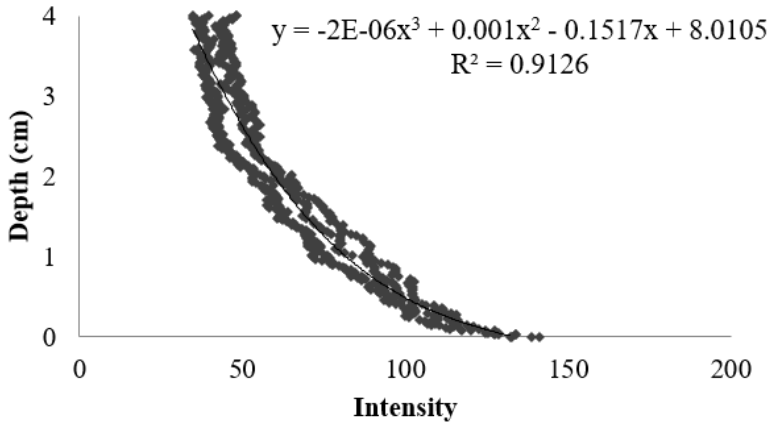

Figure 10. Example calibration curve.

Channel Velocity

I tracked channel velocity through time by collecting video footage of floating soap bubbles at each transect with Camera 2, which was mounted on the cart. The videos were converted to image sequences (30 fps) in Adobe After Effects. These videos were collected every two hours. The frames were imported as image sequences in Image-J so that bubbles could be manually traced over 20 cm vectors across each of the five transects. By knowing the frame rate, the number of frames between the vector endpoints could be used to represent time taken for the bubble to travel 20 cm (1 frame = 0.033 s), thus allowing for the calculation of velocity. To ensure that these measurements were representative of the entire channel width, a 5 x 5 cm grid was placed over the images and one measurement was taken from one bubble passing through each grid cell.

Channel Width and Bed Elevation

Terrestrial laser scanning (TLS) technology has provided the ability to quantify geomorphic change at a wide range of spatial scales by providing high-resolution topographic data. I used a Faro Focus 3-D™ laser scanner to track changes in channel

elevation and width. The scanner emits a laser beam from a rotating mirror aimed at the object of interest. The beam is reflected from the object back to the sensor, which then records distance as well as relative horizontal and vertical angles. The instrument measures relative elevations at distances between 0.6 and 130 m at a rate of up to 976,000 points per second, with a vertical range of 305° and a horizontal range of 360° (Faro, http://www.faro.com).

I placed the scanner on the cart and scanned the bed at a resolution of 1 beam per millimeter (Figure 11). Because the laser beams cannot penetrate water, the flume was drained prior to each scan so that there was no standing water in the channels. I placed Ping Pong balls at 0.5 m intervals on the lateral buffer terraces. These balls appeared in the scans and could be used to reference consecutive scans and overlay overhead images in ArcGIS. In the scanner software, Faro Scene, raw scans were trimmed of unwanted data. This included all points other than the flume surface, including buffer terraces. Trimmed scan points were then exported as ASCII (.xyz) files, where they were converted to digital elevation models (DEMs) in ArcGIS. DEMs had a resolution of 1 pixel/0.36 cm^2, and were transposed on the stitched high-resolution images for reference.

I scanned the flume every hour of flood time. Cross-sectional profiles along Transects A-E were collected from each resulting DEM. All channel elevations are in meters and are referenced to the elevation of the scanner above the flume. When channels intersected transects at angles between 45° and 90°, cross-sectional profiles were collected along the transect. If a channel intersected a transect at an angle less than 45°,

channel cross-sections perpendicular to the thalweg were extracted at the transect to avoid overestimating channel width.

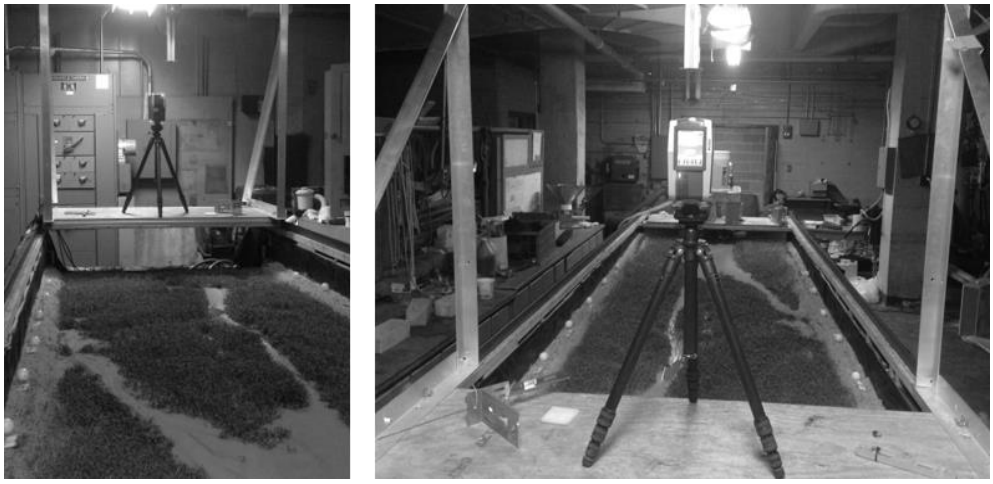

Figure 11. TLS set-up.

Fine Sediment Deposition and Floodplain Construction

In order to track changes in the spatial distribution of fine sediment during Experiment 2, I used an image processing technique used by Michal Tal (Tal and Paola, 2010). A color range threshold was applied to high-resolution overhead images of the flume from Camera 2 using a MATLAB program. This color range represented fine sediment deposits and was consistently applied to all images. Processed images show only the sediment deposits in white against a blackened flume surface.

Anticipating changes in floodplain elevation due to fine sediment deposition in Experiment 2, I manually collected cross-sectional elevation profiles of the entire flume width over Transects A-E using a point gauge at the end of each flood. A measurement was taken every 5 cm within the channel and every 5-10 cm within the floodplain. These transects allowed us to track changes in both channel and floodplain elevation

simultaneously in order to provide a measure of any sediment deposition that could be contributing to floodplain construction.

Description of Runs

I ran two experiments, one with a sediment feed consisting only of bed load material (0.5 mm sand) and one with a sediment feed consisting of bed load and suspended load (0.15 mm Clear Cut plastic sediment) at a ratio of 3:1 by weight, 1:1 by volume. Both experiments were designed for repeat floods at a constant discharge followed by 15-minute low-flow periods during which the flume was seeded at an approximated density of 1 seed/cm^2 and a six-day period for germination and growth. Each flood is referred to hereafter as a numbered "Growth Stage" (GS) that represents the approximate vegetation density. Experiment 1 lasted for seven Growth Stages, however data were only collected for six (Growth Stage 0 - Growth Stage 5). Experiment 2 lasted for 10 Growth Stages. Table 1 lists the dates, duration, and seed densities of the floods in both experiments.

Experiment 1

Growth Stage (GS)	Date	Run Time (h)	Seed Density (stems/cm²)
Growth Stage 0	7.2.15	0 - 4	0
Growth Stage 1	7.8.15	4 - 8	1
Growth Stage 2	7.14.15	8 - 12	2
Growth Stage 3	7.20.15	12 - 16	3
Growth Stage 4	7.26.15	16 - 20	4
Growth Stage 5	8.1.15	20 - 24	5
Growth Stage 6	8.7.15	24 - 28	6

Experiment 2

Growth Stage (GS)	Date	Run Time (h)	Seed Density (stems/cm²)
Growth Stage 0	9.11.15	0 - 4	0
Growth Stage 1	9.17.15	4 - 8	1
Growth Stage 2	9.23.15	8 - 12	2
Growth Stage 3	9.29.15	12 - 16	3
Growth Stage 4	10.5.15	16 - 20	4
Growth Stage 5	10.11.15	20 - 24	5
Growth Stage 6	10.17.15	24 - 28	6
Growth Stage 7	10.23.15	28 - 32	7
Growth Stage 8	10.29.15	32 - 36	8
Growth Stage 9	11.04.15	36 - 40	9

Table 1. Dates, times and seeding densities of the Growth Stages (GS) for each Experiment.

Summary of Results

I performed two flume experiments to better understand how vegetation and sediment load interact in a self-formed, gravel-bed river system as vegetation density increases. I held water discharge, sediment feed rate, slope, flood duration and seeding density constant, leaving sediment feed composition as the only variable. In Experiment 1, I used a 100% bed-load feed, and in Experiment 2 I used a 1:1 ratio of bed load and suspended load by volume. The channel geometry parameters presented in the following section refer to active channels, which I define as unvegetated channels with depths that are able to transport bedload. I referred to the Shields curve for this calculation and found that the minimum depth for transport was 2 mm.

In both experiments, channel response to the addition of vegetation agreed with the findings of previous studies. Enhanced bank strength provided by roots limited lateral mobility, reduced the number of active channels, and lowered width to depth ratios. The timescale of this response, however, varied greatly between the two experiments, as did the resulting channel dynamics. In Experiment 1, the channels initially narrowed and deepened with the introduction of vegetation. However, the channel network in the upper 2m of the flume began to aggrade after only two floods as channel banks strengthened and roughness increased. Within the first three floods, the single remaining active channel became choked with bed material, diverting flow overbank into the floodplain. Lobes of sand collected at the active channel margins, burying floodplain vegetation. As a result, there was very little lateral channel movement in Experiment 1, and the result was a single straight channel, of which the upper 3.5 m had been filled with bed material.

This aggradation starved the lower portion of the channel of bed load, causing scour. By the end of Experiment 1, all discharge in the upper 3.5 m of the flume had been diverted into the floodplain, the topography of which remained largely unchanged with the exception of the sand levees that developed along the channel margins.

The channel network in Experiment 2 evolved much differently in response to increasing vegetation density. I observed a slower transition from a multi-thread to a single-thread channel network, compared with Experiment 1. The primary mechanism for channel adjustment shifted from "sweeping" back and forth across the floodplain to avulsions between individual active channels. Active channel aggradation was not observed in Experiment 2 until GS 6, when the single remaining channel was fully constrained on either side by vegetation. Until GS 6, 100% of discharge to the flume was carried by the active channel, as opposed to being partially or fully diverted into the floodplain in Experiment 1. This provided the channel with enough stream power to erode vegetated banks and build alternate bars – which I did not observe during Experiment 1. Once channel aggradation initiated overbank flow, I observed deposits of plastic sediment deep within the floodplain, filling in depressions that had been earlier low-flow channels in addition to chute cutoffs. The resulting morphological characteristics from vegetation-sediment interactions during overbank flow conditions are the primary differences between the two experiments.

Experiment 1 Results

Detailed Observations

The following is a description of detailed observations of channel evolution throughout Experiment 1, broken into phases of similar behavior.

Phase I. GS0 – GS1: In the absence of vegetation, the initial channel widened and braided, shifting unconstrained across the floodplain (Figure 12). During GS 1 (GS1), low-density vegetation establishment on exposed bars stabilized isolated areas. The channel(s) avulsed around these bars rather than sweeping freely across the floodplain (Figure 13).

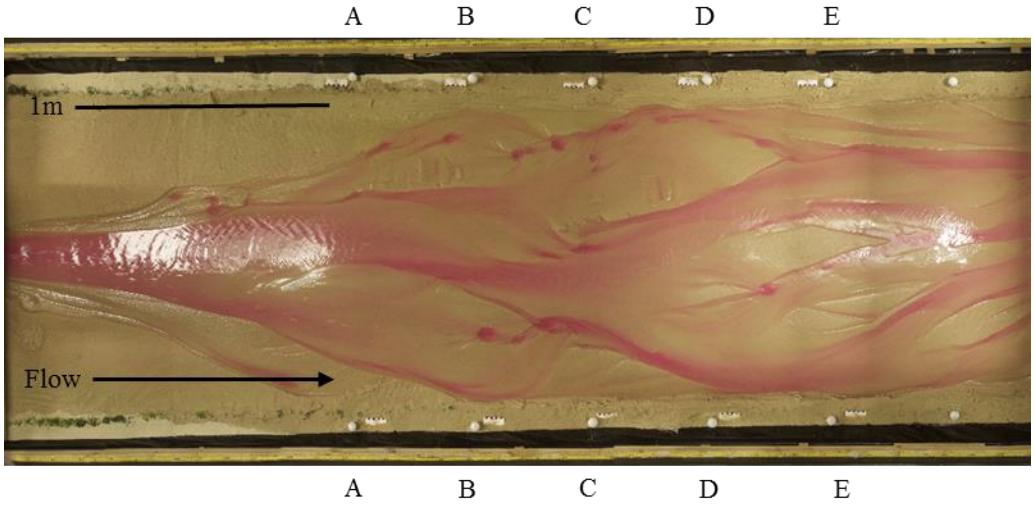

Figure 12. Experiment 1, end of GS0.

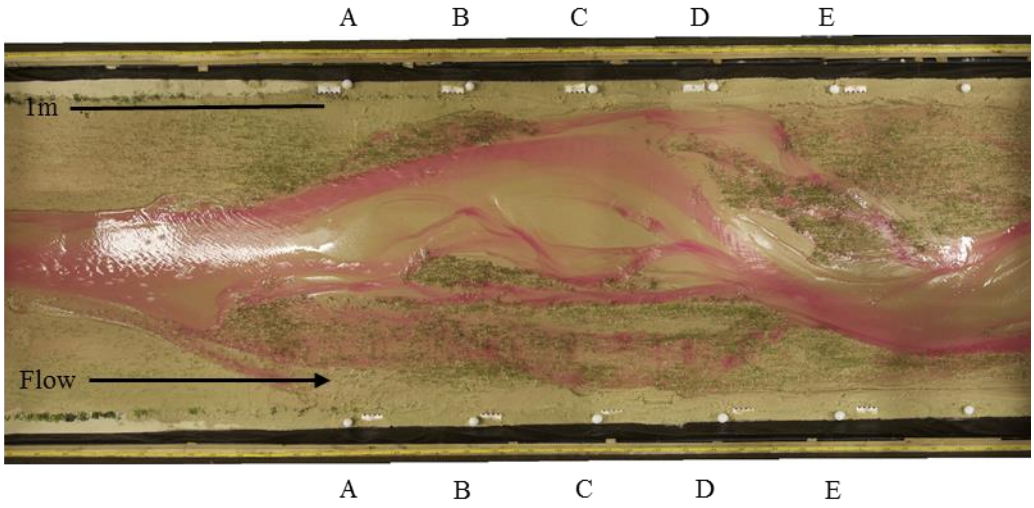

Figure 13. Experiment 1, end of GS1.

Phase II. GS2 – GS3: Vegetation established in weaker channels and on exposed bars, limiting total channel width and mobility. As vegetation choked off abandoned or low-flow channels, flow consolidated into fewer and fewer channel threads until two active channels remained. In the upper 2.5 m of the flume, these two channels began to aggrade during GS2, fixing the channel boundaries and forcing flow overbank into the floodplain (Figure 14). By the end of GS 3 (Figure 15), one of the two remaining channels became choked with vegetation and there remained one single, straight channel, the upper 3.0 m of which is only 5-7 cm wide. The majority of discharge was routed through the floodplain around the aggraded area, and re-joined the active channel at Transect D, where a large scour hole (2-3 cm deep) developed.

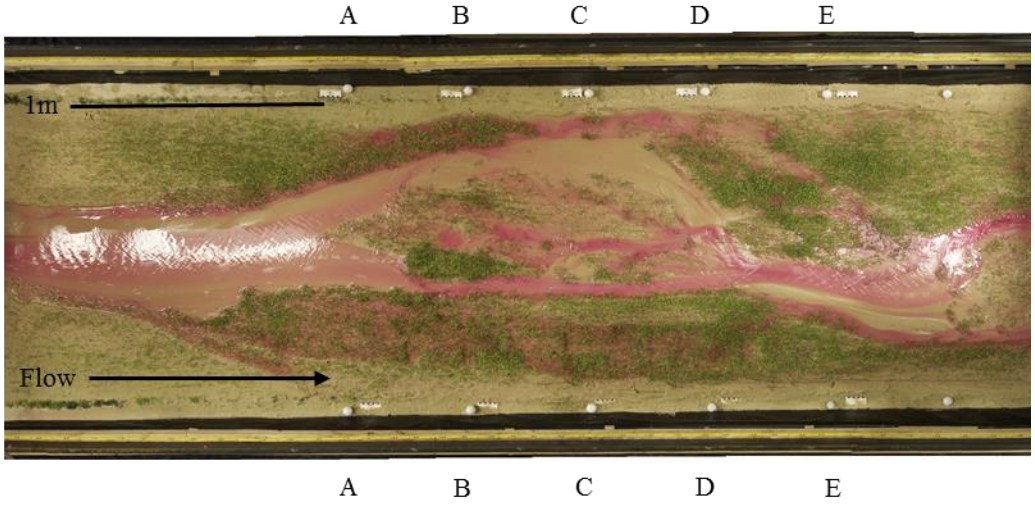

Figure 14. Experiment 1, end of GS2.

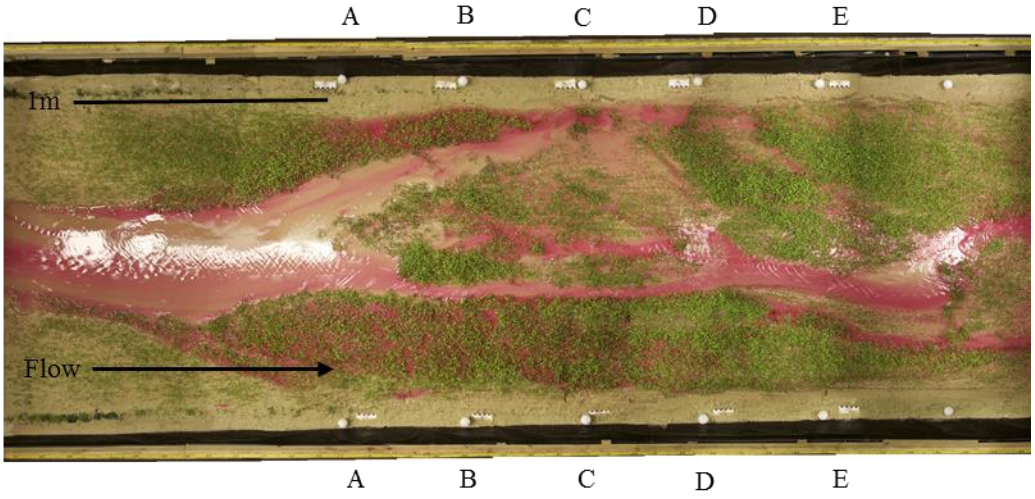

Figure 15. Experiment 1, end of GS3.

Phase III. GS4 – GS5: The active channel continued to aggrade between Transects A and D. Lobes of sand deposited in the active channel began to encroach into the floodplain in this area, burying vegetation. White circles in Figure 16 indicate where sand levees begin to develop along the channel margin. The average depth of flow in the floodplain was 1.2 cm. By the end of GS 5 (Figure 17), the channel between transects B and D had been completely abandoned, exposing it to vegetation encroachment at the

next seeding. The white circle in Figure 17 indicates where the channel has been abandoned.

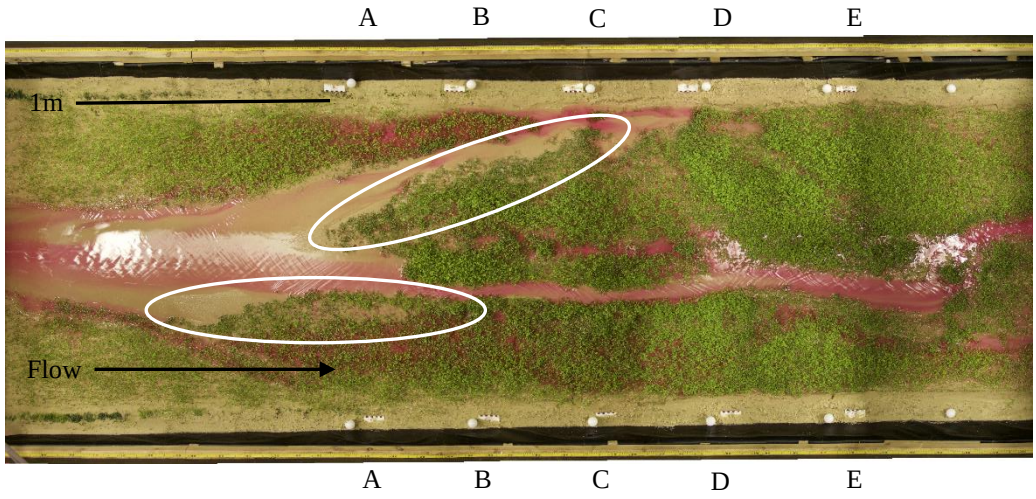

Figure 16. Experiment 1, end of GS4.

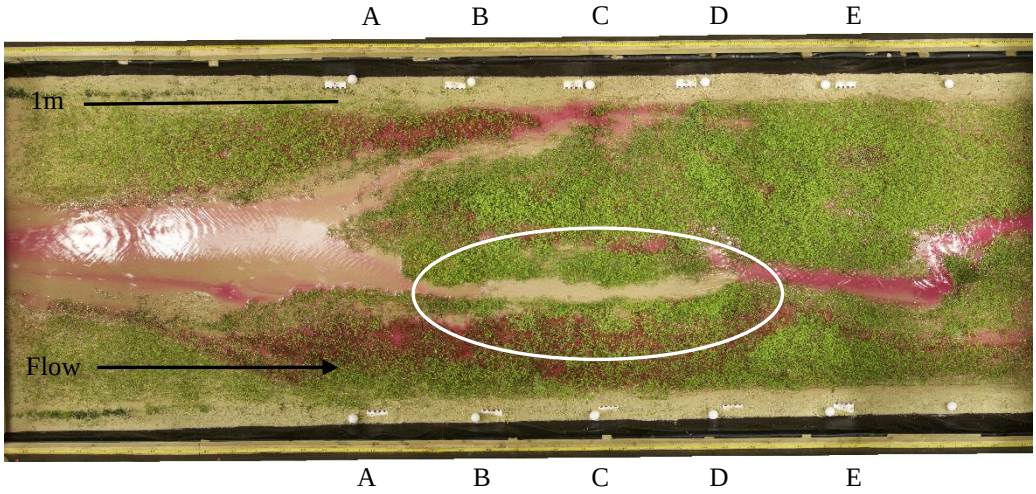

Figure 17. Experiment 1, end of GS5.

Phase IV. GS6: Vegetation covered the entire active channel between Transect B and D during the final flood (Figure 18), prohibiting the collection of active channel flow data. The average depth (measured directly) in the floodplain had increased to 1.5 cm. Prolonged inundation of the floodplain ultimately killed vegetation, clearing flowpaths. White lines in Figure 18 indicate major flow paths through the floodplain.

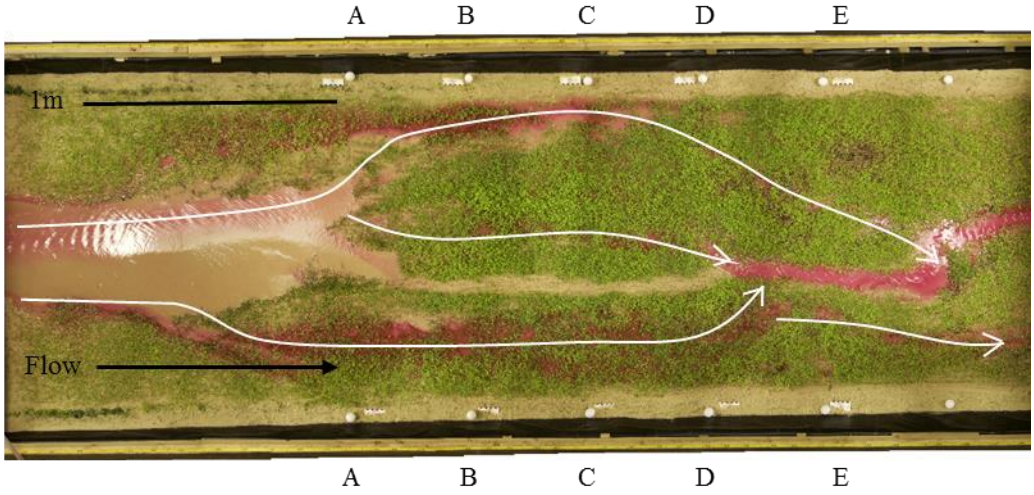

Figure 18. Experiment 1, end of GS6.

Channel Width

Average active channel width decreased from 62 cm to 12 cm over the course of Experiment 1 (Figure 19). Across all five transects, channel width declined substantially in response to vegetation encroachment between GS1 and GS2. When aggradation in the upper 2.5 m of the channel forced flow into the vegetated floodplain, channel width stabilized between Transects B and E, while the channel with at Transect A remained wider and variable through time.

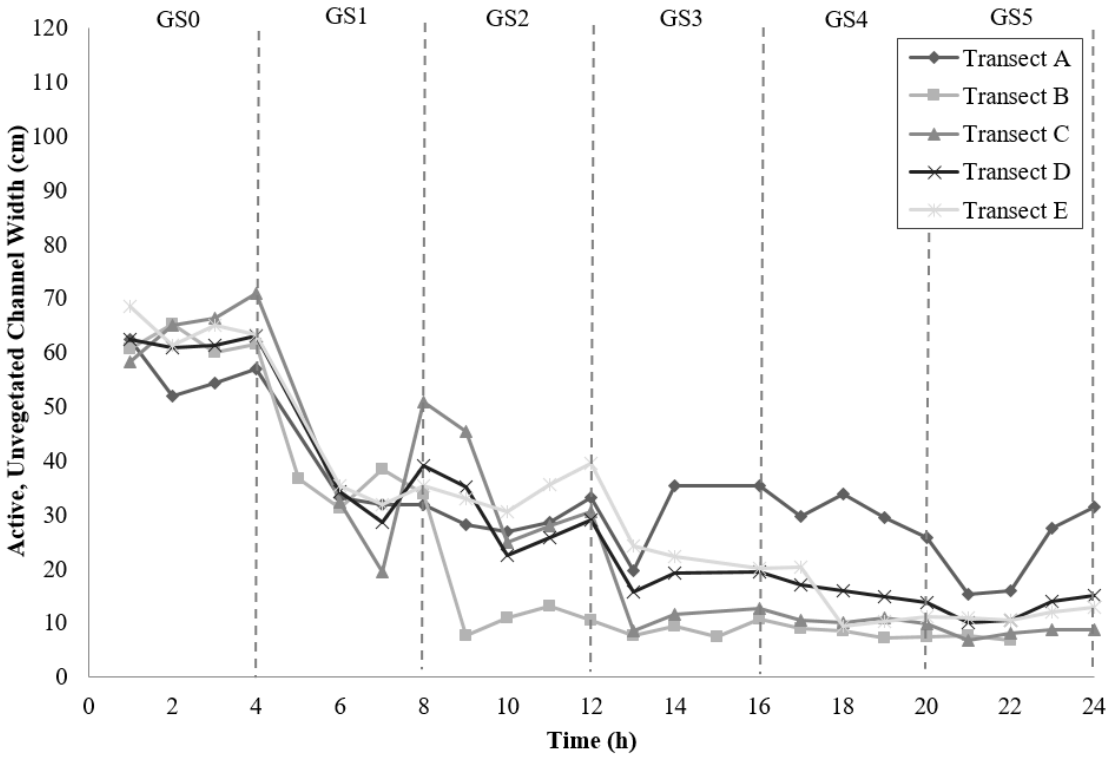

Figure 19. Experiment 1 average widths.

Channel Depth

Change in active channel depth through time varied longitudinally during Experiment 1 (Figure 20). Average channel depth increased initially between Transects A-C (2.0 – 3.0 m downstream from headwall), then began to decline after GS2. By contrast, downstream of the aggraded area between Transects A and C, Transects D and E nearly tripled in depth over the course of the experiment. Flood-averaged channel depth at each transect, with standard deviation, is displayed in Table 2. The standard deviation from mean depth represents the distribution of depth measurements across the cross-sectional channel profile. Standard deviation values throughout the experiment follow a trend similar to depth.

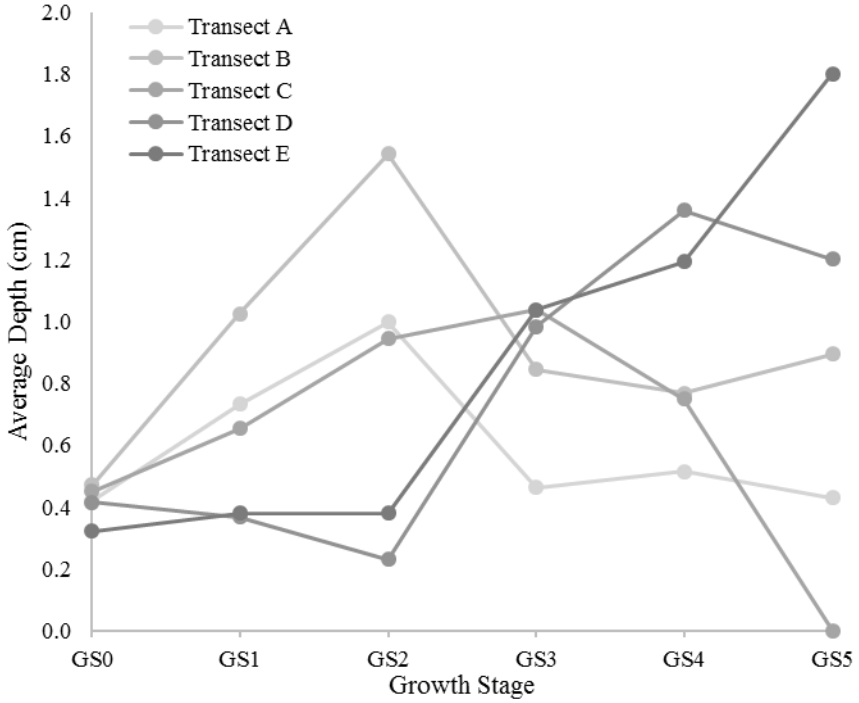

Figure 20. Experiment 1 average depths.

Transect	GS0	GS1	GS2	GS3	GS4	GS5
A	0.4, 0.2	0.7, 0.5	1.0, 0.6	0.5, 0.2	0.5, 0.4	0.4, 0.3
B	0.5, 0.5	1.0, 0.4	1.5, 0.4	0.8, 0.4	0.8, 0.5	0.9, 0.3
C	0.4, 0.2	0.7, 0.3	0.9, 0.3	1.0, 0.7	0.7, 0.4	0.0, ---
D	0.4, 0.3	0.4, 0.2	0.2, 0.1	1.0, 0.5	1.4, 0.4	1.2, 0.8
E	0.3, 0.2	0.4, 0.2	0.4, 0.2	1.0, 0.7	1.2, 0.3	1.8, 0.3

Table 2. Experiment 1 average depths in centimeters with standard deviation.

Channel Velocity

Mean surface flow velocities increased from 31 cm/s to 37 cm/s over the course of Experiment 1 (Figure 21). By the end of GS 5, the active channel had been completely abandoned and no velocity measurements could be made in this area. For this reason, the total number of velocity data points for Experiment 1 is smaller than that of Experiment 2. During GS5 of Experiment 1, active channel velocity measurements could only be made on Transects D and E, where flow through the vegetated floodplain on each side of

the flume re-entered the active channel. This is likely the reason for the increase in mean channel velocity during this stage. Overall, there is no observable trend in mean channel velocity during Experiment 1.

The frequency distribution of binned velocity measurements is shown in Figure 22. Remember that the number of measurements, defined as n, decreases with each successive flood because I measured one bubble for every 5 cm of channel width across each of the five transects. As demonstrated earlier, channel width decreased with vegetation encroachment, and therefore so must n. While the overall trend in mean channel velocity may not be significant, the frequency distribution shows a progressive shift in the data from each individual flood towards higher velocity 'bins' from GS0-GS5.

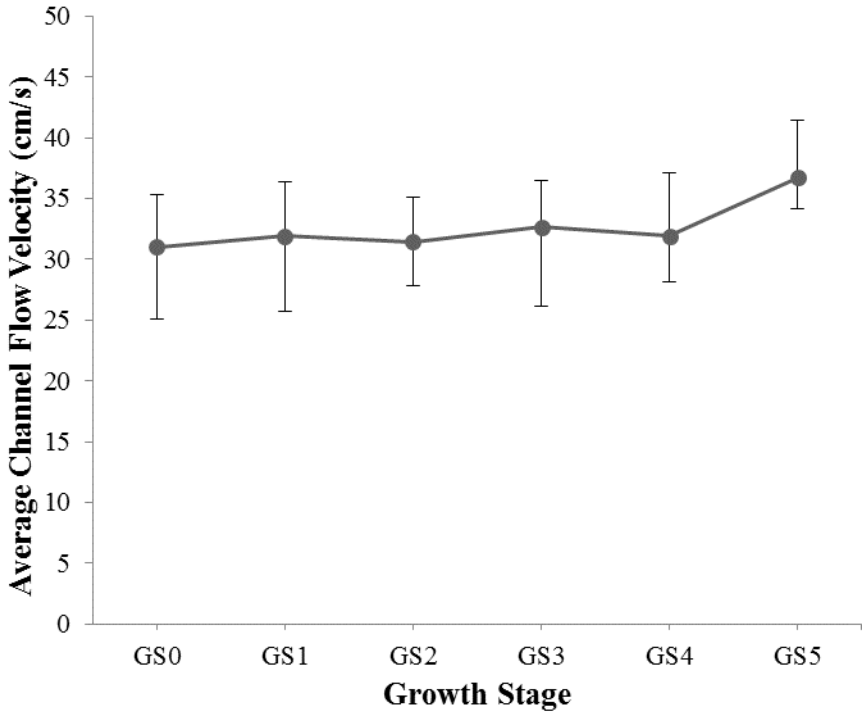

Figure 21. Experiment 1 average surface velocity with standard deviation.

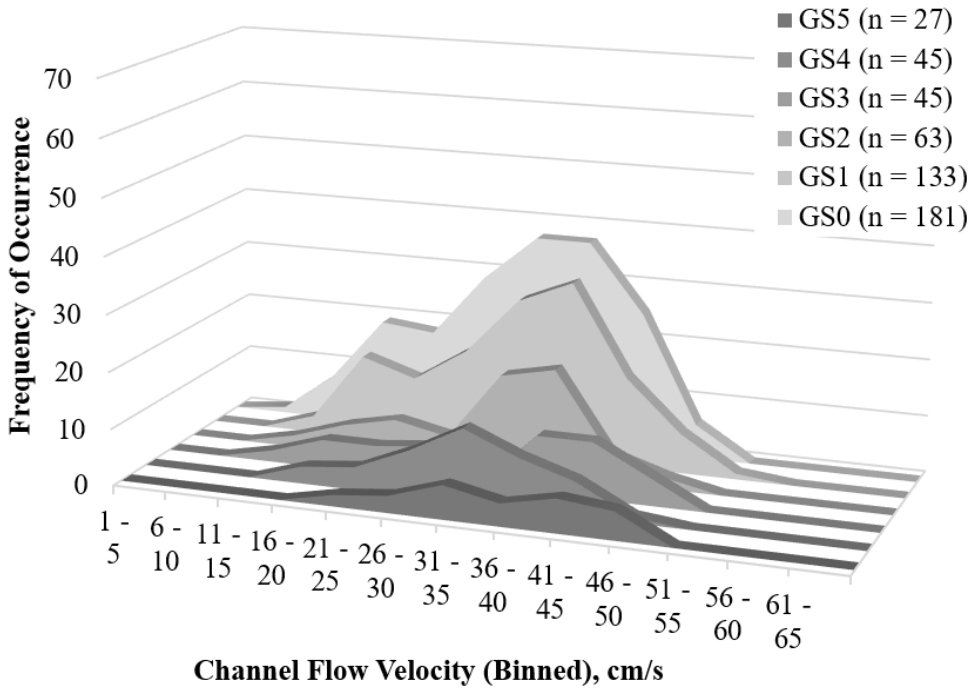

Figure 22. Experiment 1 frequency distribution of velocity measurements.

Channel Elevation and Geometry

Minimum elevation of the active channel(s) through time is displayed in Figure 23. All transects show a slight (0.2-0.5 cm) downcutting of the bed during GS1. After GS 1, however, the bed elevation of Transects A begins to rise, followed by Transect B, and then C. At the end of GS 5, the minimum channel elevations of transects A, B and C are at least 2 cm higher than they were at the end of GS 0. By contrast, Transect D is 2 cm *lower* at the end of GS 5. Overall, changes in minimum channel elevation during Experiment 1 vary with distance from the headwall.

Figures 24-28 display active channel cross-sections across Transects A-E, which shows changes in bed elevation as well as channel shape through time. These profiles were extracted DEMs of lidar scans of the flume at the end of every flood, just before

seeding. They indicate channel narrowing over time as vegetation density increases. Also, they show major aggradation between Transects A and C while transects D and E progressively narrow and deepen through time. Using flood-averaged width and depth measurements, I calculated width to depth ratios, displayed in Table 3 which further demonstrate a narrowing of channels in response to increasing vegetation density.

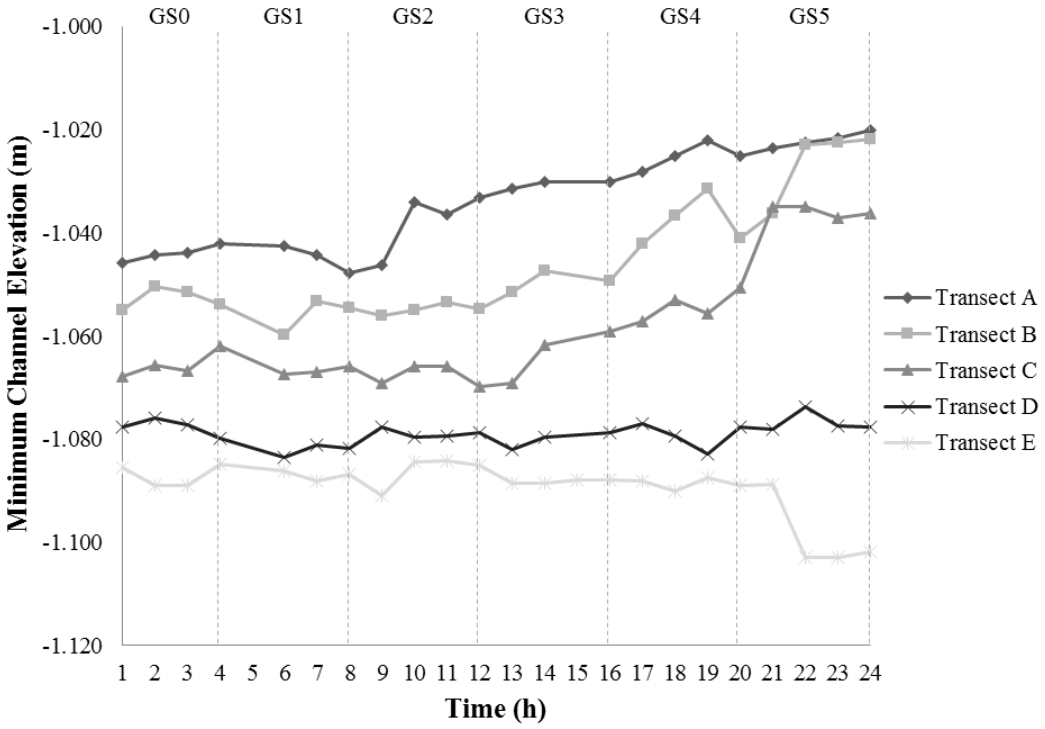

Figure 23. Experiment 1 minimum channel elevations.

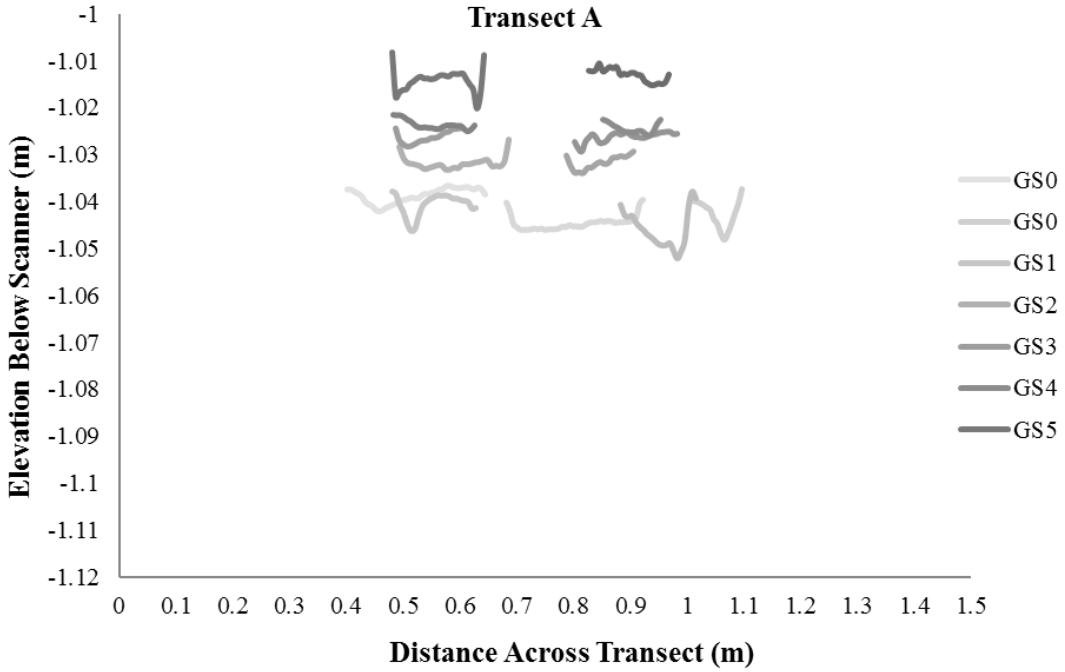

Figure 24. Experiment 1, Transect A elevation profiles.

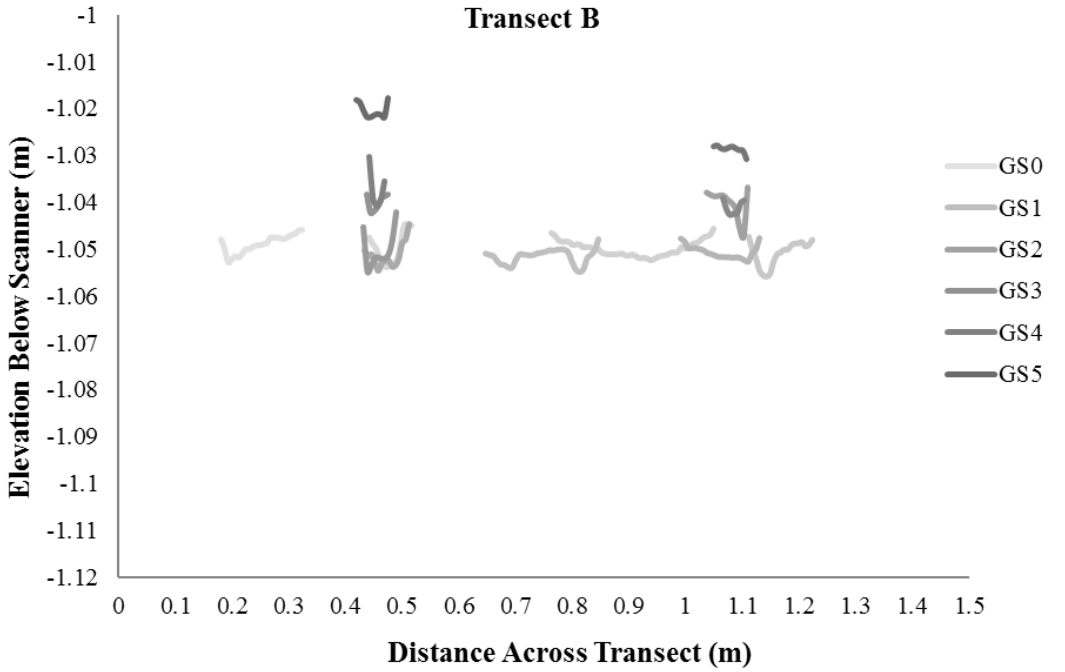

Figure 25. Experiment 1, Transect B elevation profiles.

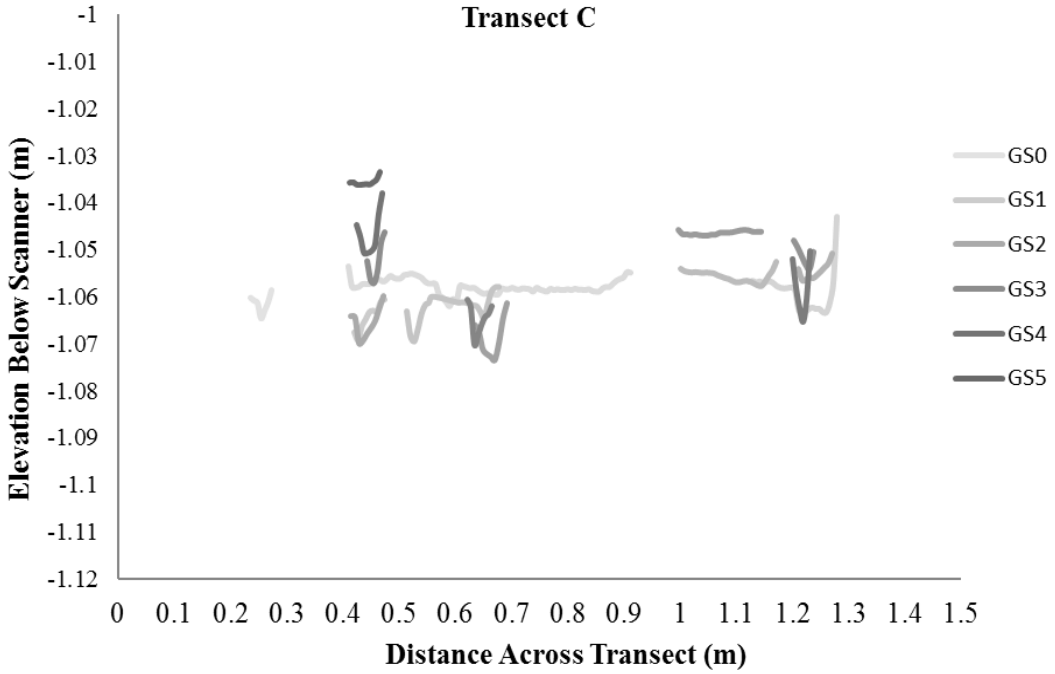

Figure 26. Experiment 1, Transect C elevation profiles.

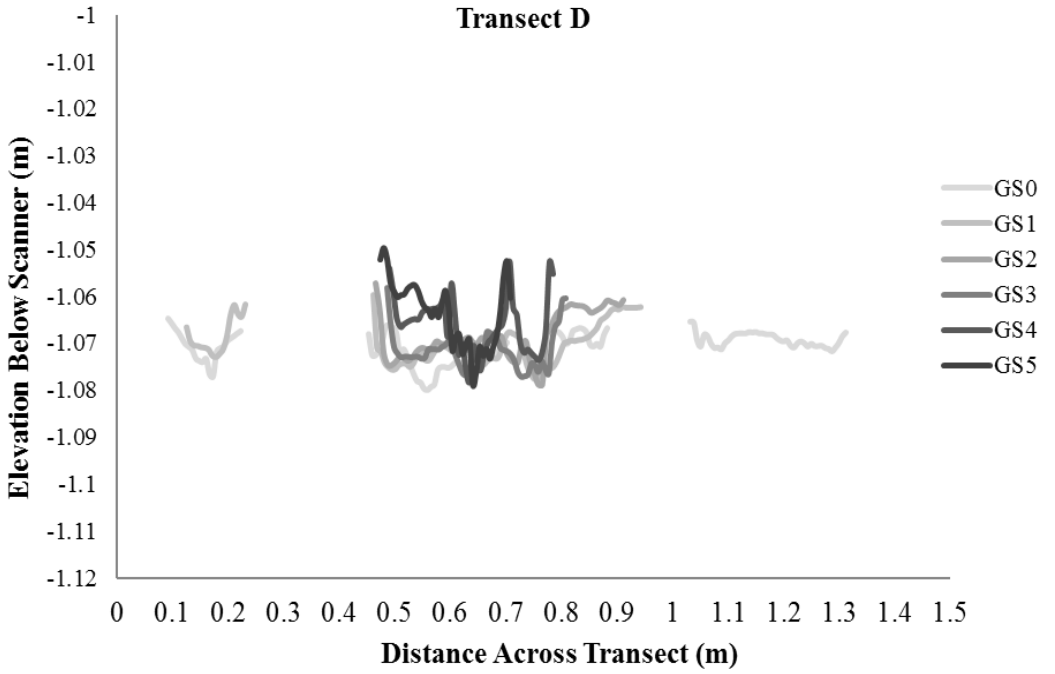

Figure 27. Experiment 1, Transect D elevation profiles.

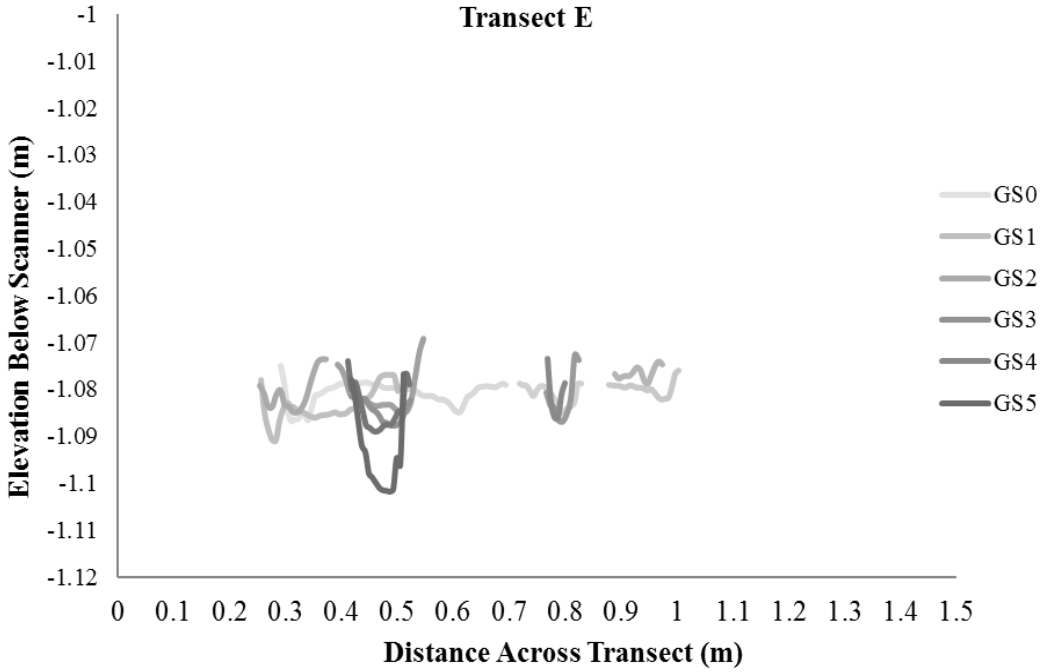

Figure 28. Experiment 1, Transect E elevation profiles.

Transect	GS0	GS1	GS2	GS3	GS4	GS5
A	140.9	44.6	29.5	59.9	59.3	56.4
B	123.7	35.0	7.0	10.9	11.7	8.0
C	162.6	52.8	30.9	10.8	14.6	---
D	154.9	85.7	128.8	17.8	10.6	10.3
E	215.2	84.7	88.0	21.7	8.5	6.4

Table 3. Experiment 1 width to depth ratios.

Experiment 2 Results

Detailed Observations

The following is a description of detailed observations of channel evolution throughout Experiment 2, broken into phases of similar behavior.

Phase I. GS0 – GS1: In the absence of vegetation, the initial channel widened and braided, shifting unconstrained across the floodplain (Figure 29). During GS1, low-

density vegetation establishment on exposed bars stabilized isolated areas. The channel(s) avulse around these bars rather than sweeping freely across the floodplain (Figure 30).

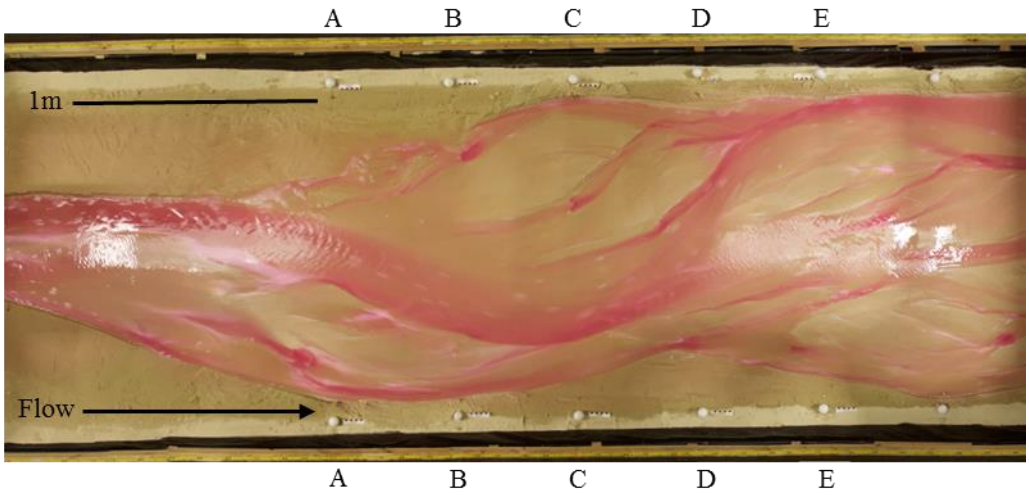

Figure 29. Experiment 1, end of GS0.

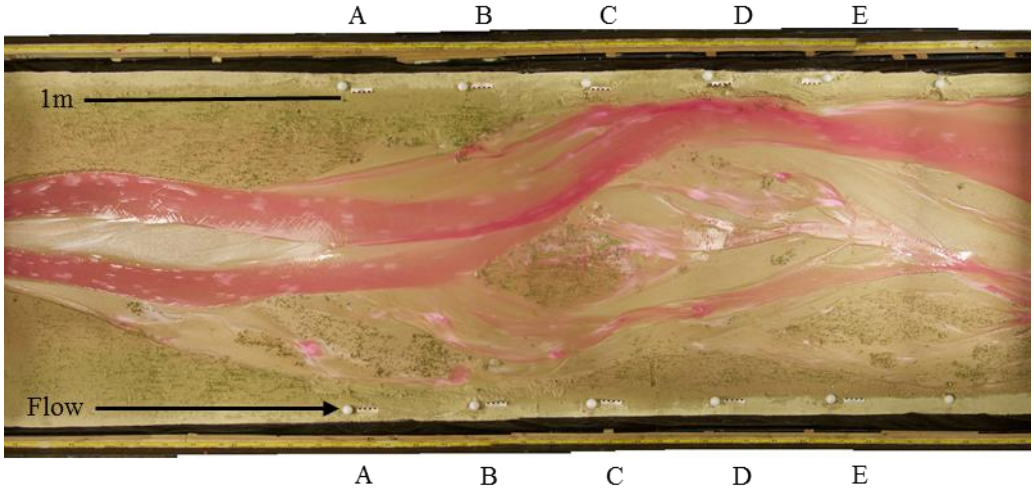

Figure 30. Experiment 2, end of GS1.

Phase II. GS2 – GS3: Vegetation established in weaker channels and on exposed bars, limiting total channel width and mobility. As vegetation chokes off abandoned or low-flow channels, flow is consolidated into fewer and fewer channel threads until a single active channel remains (Figures 31, 32).

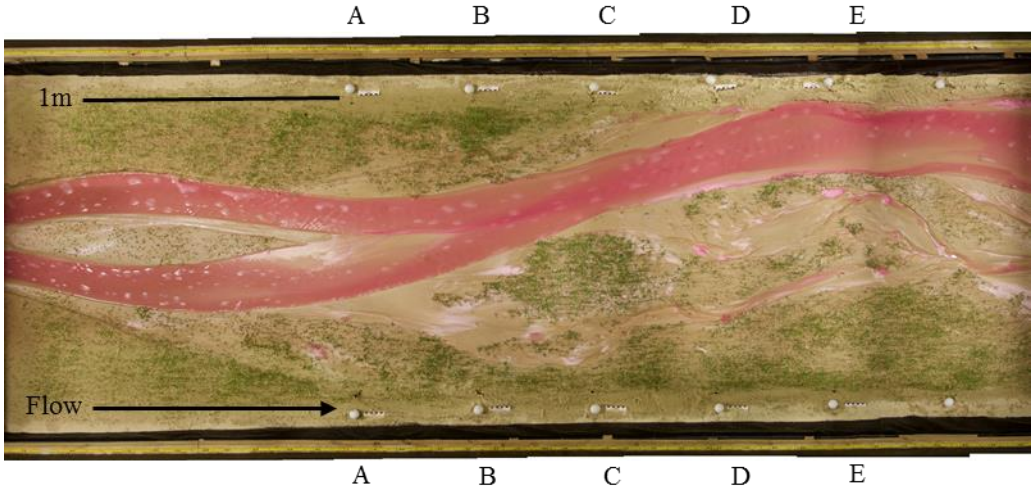

Figure 31. Experiment 2, end of GS2.

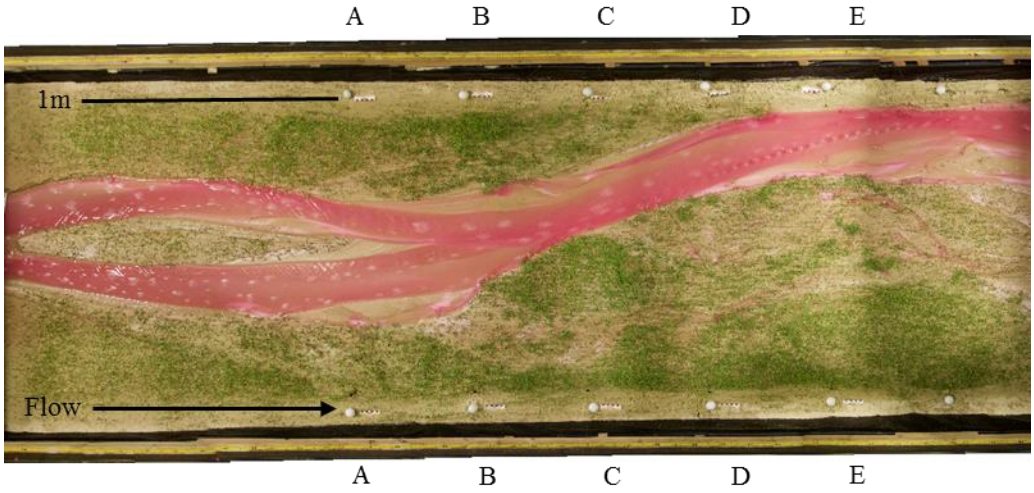

Figure 32. Experiment 2, end of GS3.

Phase III. GS4 – GS5: Further flow consolidation leads to the erosion of vegetated banks and the generation and growth of alternate bars (Figure 33), where fine sediment began to accumulate. By GS5, vegetation began to occupy new bars generated during GS4 (Figure 34).

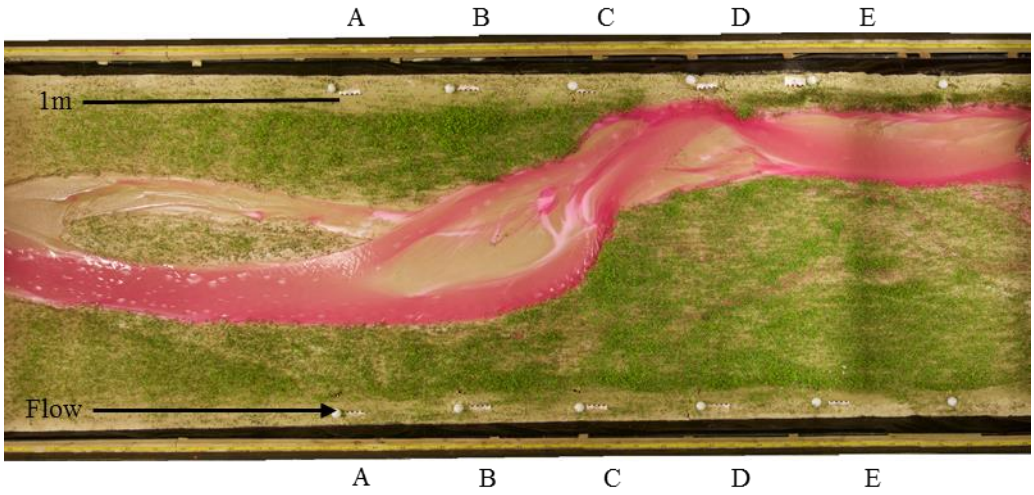

Figure 33. Experiment 1, end of GS4.

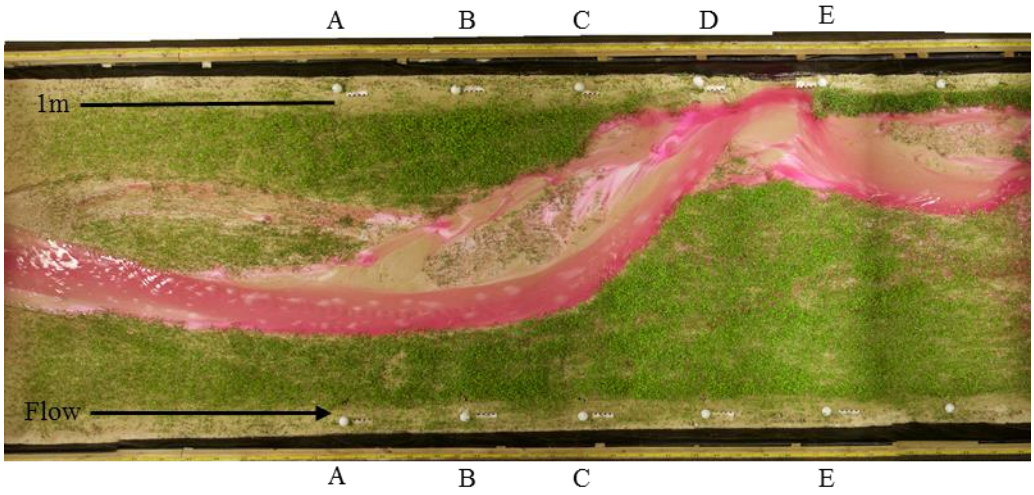

Figure 34. Experiment 2, end of GS5.

Phase IV. GS6 – GS7: Meander bends continue to grow during GS6 as bars are strengthened by vegetation. A channel cutoff develops at Transect E during GS7. The channel begins to aggrade towards the end of GS6 (Figure 35), overtop its banks and spill into the floodplain, re-occupying former low-flow channels. Fine sediment begins to collect in floodplain channels and channel cutoffs, which is evident in Figure 36.

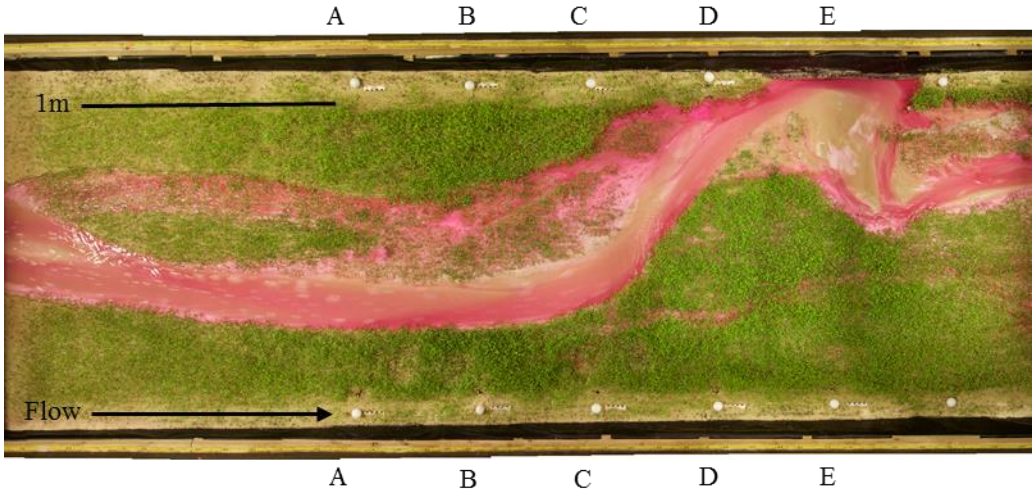

Figure 35. Experiment 2, end of GS6.

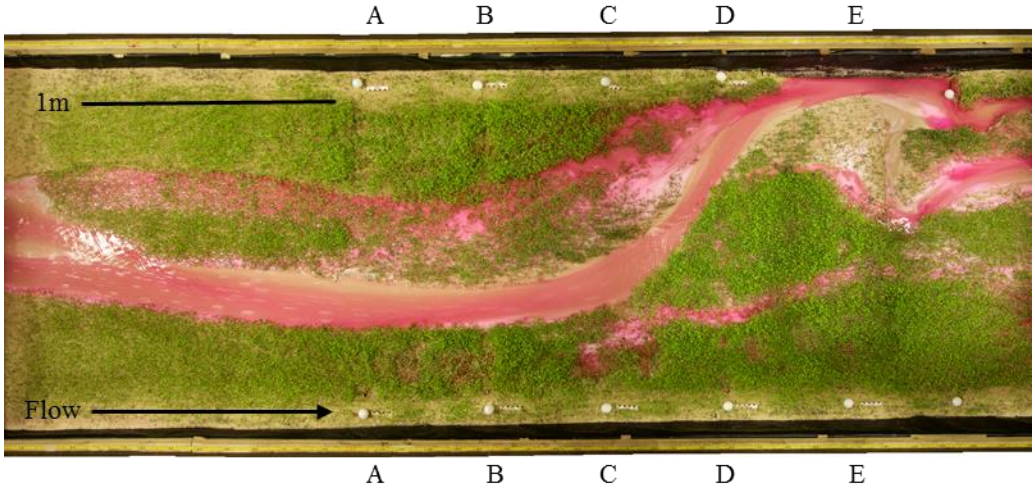

Figure 36. Experiment 2, end of GS7.

Phase V. GS8 – GS9: Fine sediment fills floodplain depressions (Figure 37), including old channels and chute cutoffs. High vegetation density limits the rate of bar growth to rate of bank erosion, similar to the behavior of fully-developed meandering channels. The channel has eroded a lateral buffer and now flows along the bare wall (Figures 37 and 38).

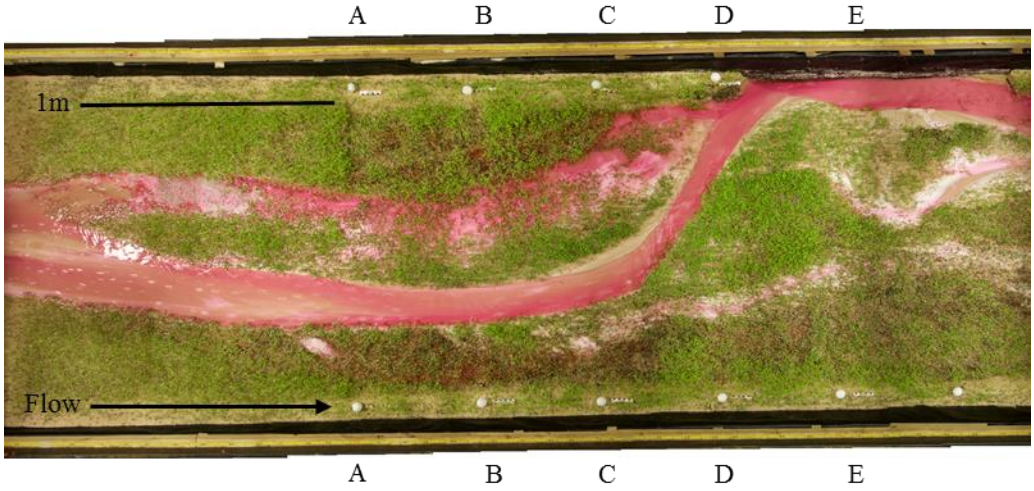

Figure 37. Experiment 2, end of GS8.

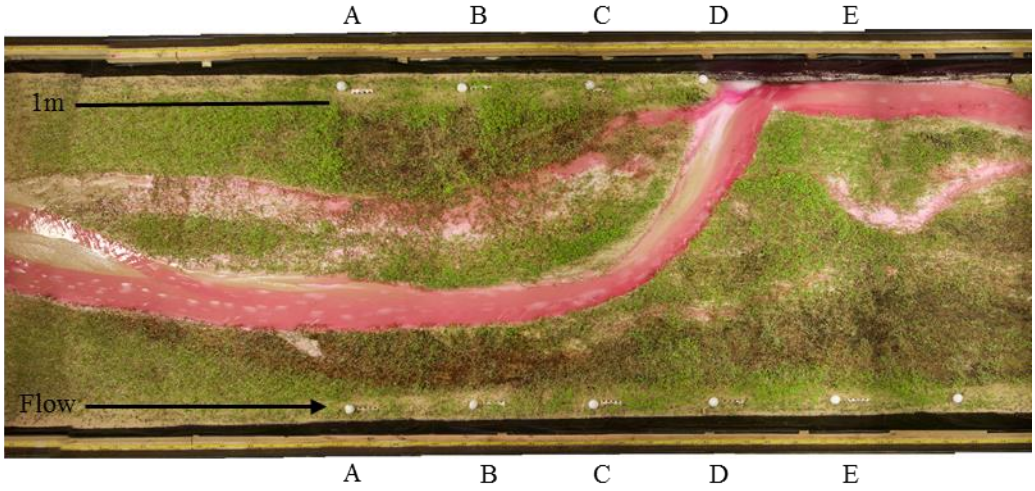

Figure 38. Experiment 2, end of GS9.

Channel Width

Average channel width decreased from 85 cm to 25 cm over the course of Experiment 2. Across all five transects, channel width declined substantially in response to vegetation encroachment between GS1 and GS3. During GS4, the channel became fully consolidated into a single thread. Once consolidated, the channel began to erode its banks, widen, and develop mid-channel bars. This re-widening is reflected in the abrupt

increases in channel width during GS4 and the beginning of GS5 (Figure 39). During GS5, however, the weaker channel that flowed around the mid-channel bar was abandoned during an avulsion. After GS5, the channel became single-thread once again, but with banks that were re-fortified by continued seeding. At this stage, channel width remained relatively stable for the remainder of the experiment.

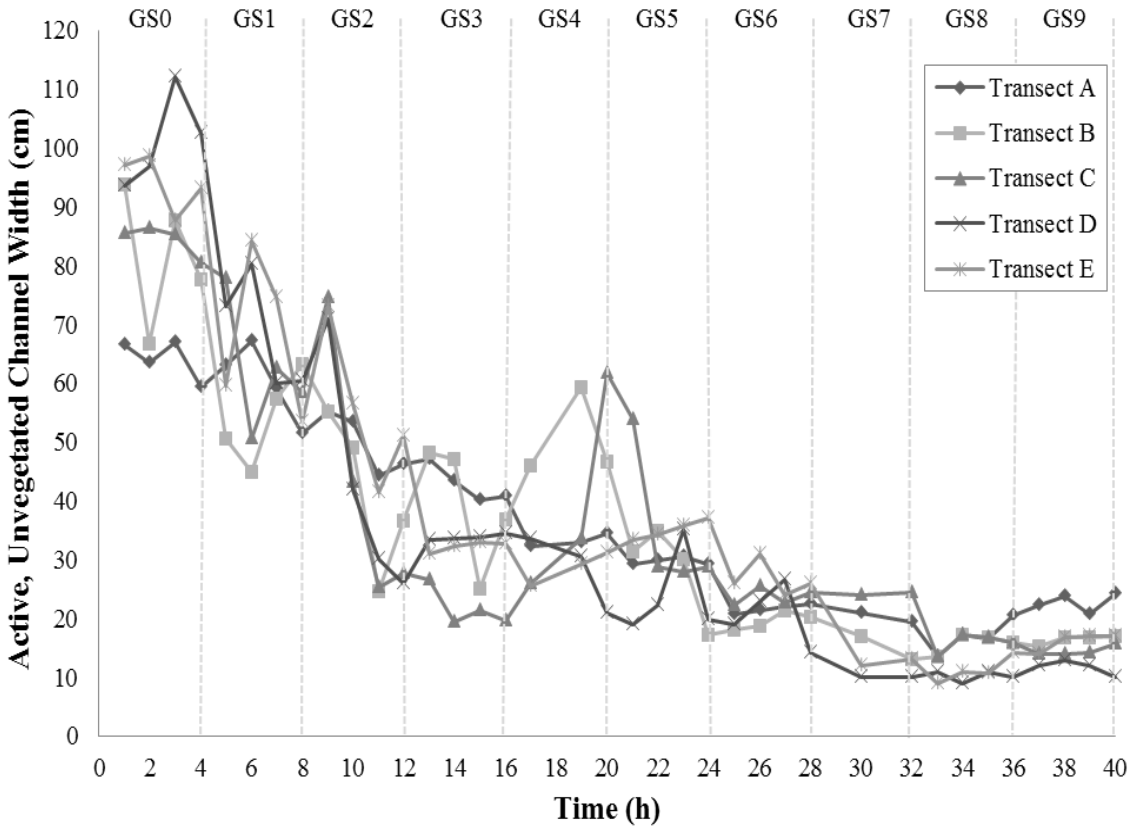

Figure 39. Experiment 2, average channel width

Channel Depth

Among all transects, average channel depth increased from 0.4 cm to 0.8 cm over the course of Experiment 2. Average channel depth increased between GS1 and GS5 (Figure 40), at which point channel banks were fully vegetated. However, channel depth

began to decline towards the end of GS6 and throughout GS7, in conjunction with some aggradation of the channel bed. After GS7, average depth appears to stabilize. Standard deviation from mean depth (Figure 41) represent the distribution of depth measurements across the cross-sectional channel profile. Standard deviation values throughout the experiment follow a trend similar to depth.

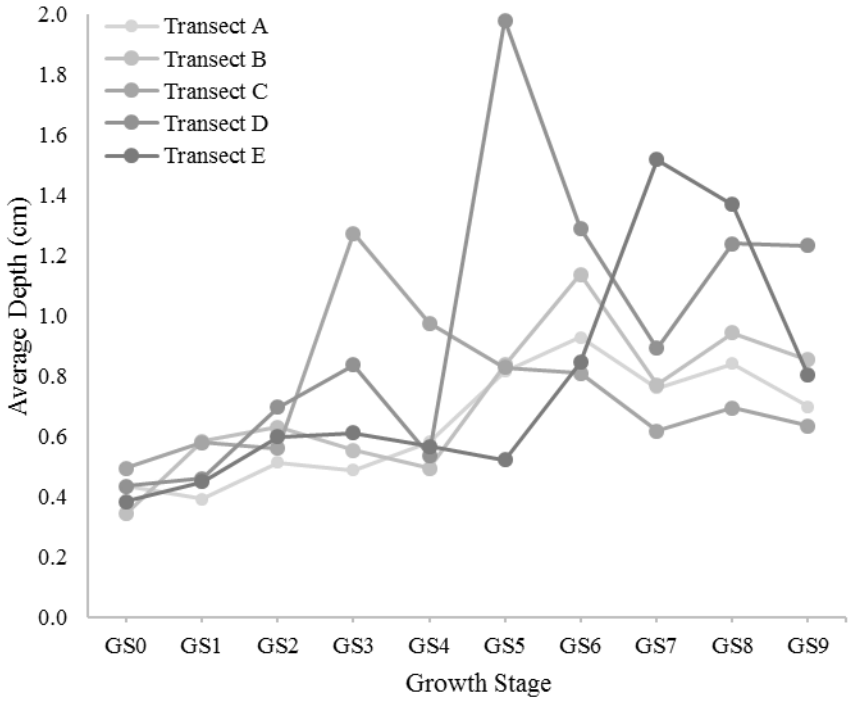

Figure 40. Experiment 2 average depths.

Transect	GS0	GS1	GS2	GS3	GS4	GS5	GS6	GS7	GS8	GS9
A	0.4, *0.2*	0.4, *0.2*	0.5, *0.1*	0.5, *0.3*	0.6, *0.3*	0.8, *0.3*	0.9, *0.3*	0.8, *0.3*	0.8, *0.5*	0.7, *0.3*
B	0.3, *0.1*	0.6, *0.4*	0.6, *0.2*	0.6, *0.3*	0.5, *0.2*	0.8, *0.4*	1.1, *0.3*	0.8, *0.2*	0.9, *0.3*	0.9, *0.3*
C	0.5, *0.3*	0.6, *0.4*	0.6, *0.3*	1.3, *0.6*	1.0, *0.6*	0.8, *0.5*	0.8, *0.5*	0.6, *0.3*	0.7, *0.2*	0.6, *0.4*
D	0.4, *0.3*	0.5, *0.2*	0.7, *0.4*	0.8, *0.4*	0.5, *0.4*	2.0, *0.9*	1.3, *0.8*	0.9, *0.5*	1.2, *0.8*	1.2, *0.6*
E	0.4, *0.2*	0.5, *0.2*	0.6, *0.4*	0.6, *0.6*	0.6, *0.4*	0.5, *0.5*	0.8, *0.6*	1.5, *0.9*	1.4, *0.7*	0.8, *0.4*

Table 4. Experiment 2 average depth in centimeters with standard deviation

Channel Velocity

Mean surface flow velocities increased from 30 cm/s to 42 cm/s over the course of Experiment 2 (Figure 42) GS0 and GS1 had the same average channel flow velocities, 30 cm/s. Figure 43 shows the frequency distribution of all velocity measurements for each flood. Remember that the number of measurements, n, decreases with each successive flood because I measured one bubble for every 5 cm of channel width across each of the five transects. As demonstrated earlier, channel width decreased with vegetation encroachment throughout the experiment, and therefore so must n. As the channel network consolidates into fewer, narrower channels, I see that the distribution of the data shifts from a bimodal distribution in GS0 and GS1 to a unimodal distribution shifted towards higher surface velocities.

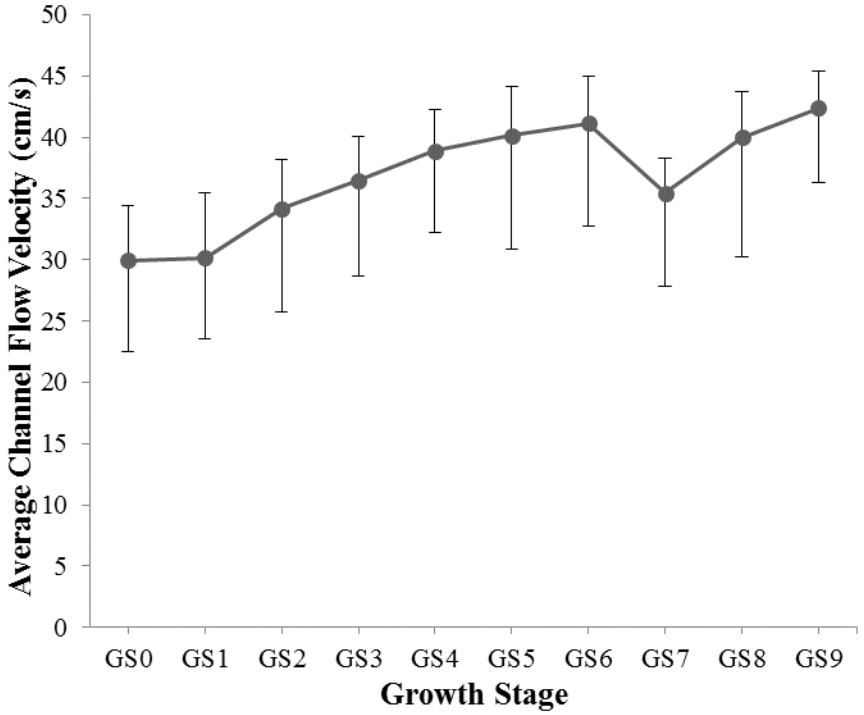

Figure 41. Experiment 2 average surface flow velocities with standard deviation.

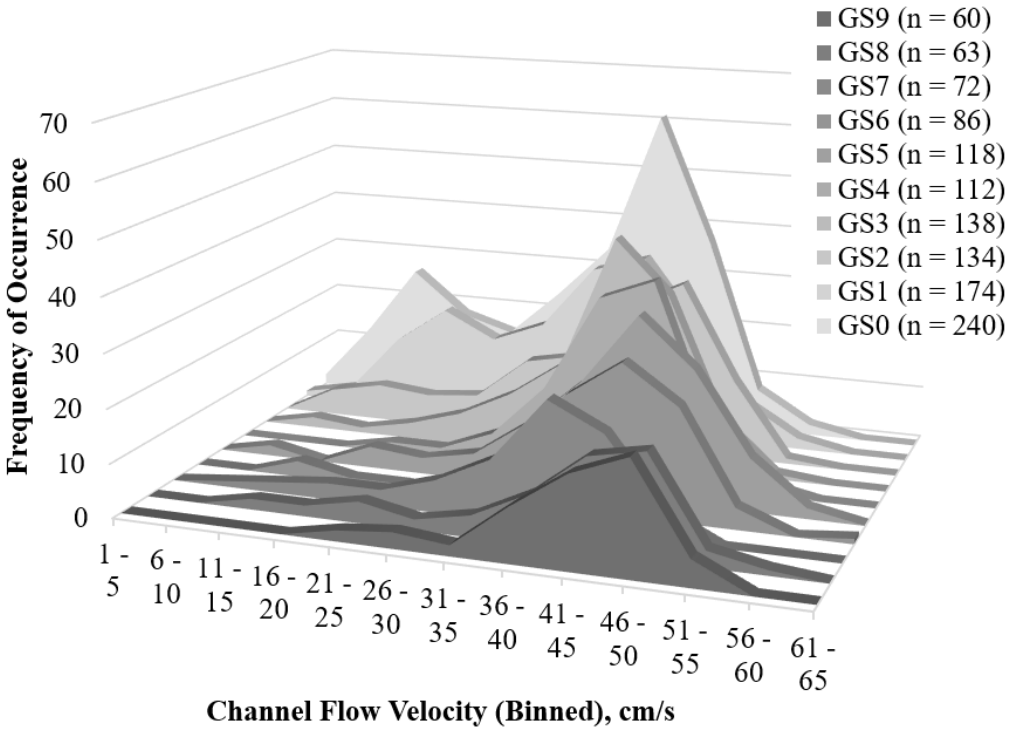

Figure 42. Experiment 2 frequency distribution of velocity measurements.

Channel Bed Elevation and Geometry

Minimum elevations of the active channels through time are displayed in Figure 44. Across all transects, the minimum elevation begins to decline during GS2. This trend persists until the second half of GS4. At this point, the minimum elevation of the active channel across Transects A-C begins to aggrade. Transect D follows suit beginning in GS6. Transect E shows no signs of aggradation, rather the minimum channel elevation unsteadily continues to decrease after GS1.

Figures 45-49 show cross-sectional profiles of the unvegetated channels across Transects A-E through time. In all transects, the transformation of channel geometry from wide, shallow channels to narrow, deeper channels is evident in all five transects. These

transects also highlight the aggradation that occurs in Transects A-D. Using flood-averaged width and depth measurements, I calculated width to depth ratios, displayed in Table 4, which further demonstrate a narrowing of channels in response to increasing vegetation density.

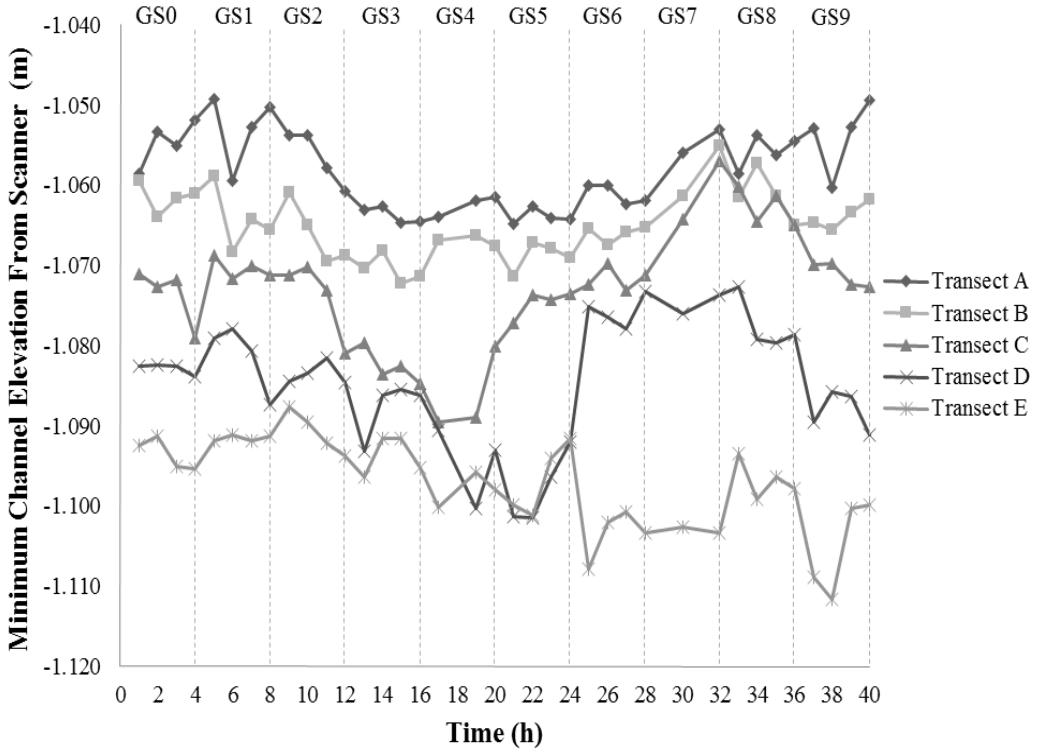

Figure 43. Experiment 2 minimum channel elevation.

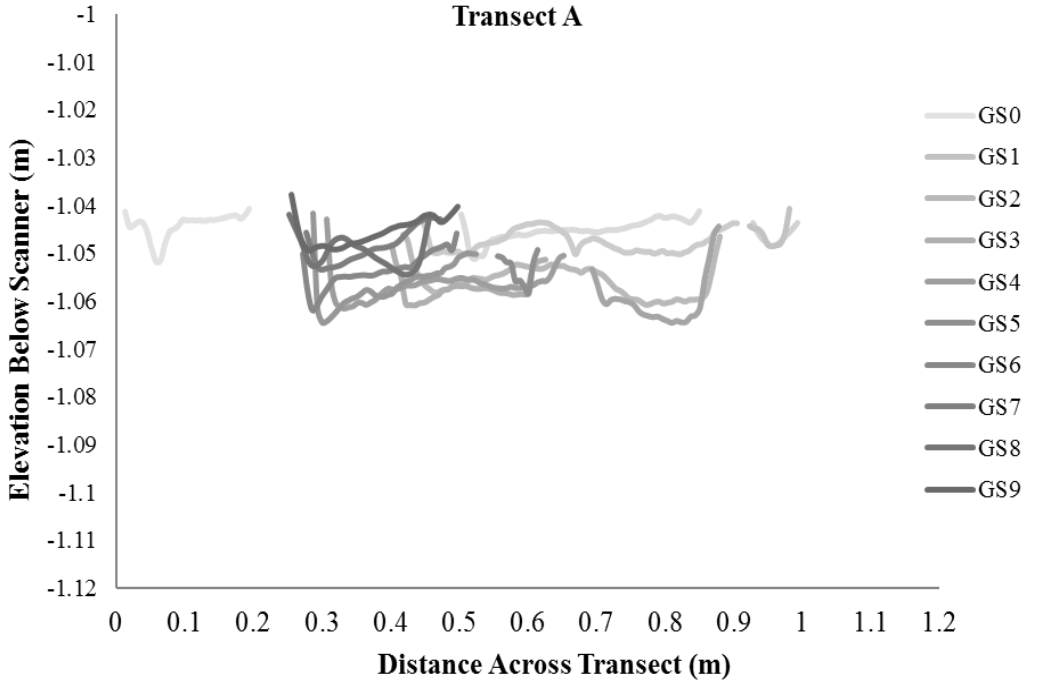

Figure 44. Experiment 2, Transect A elevation profiles.

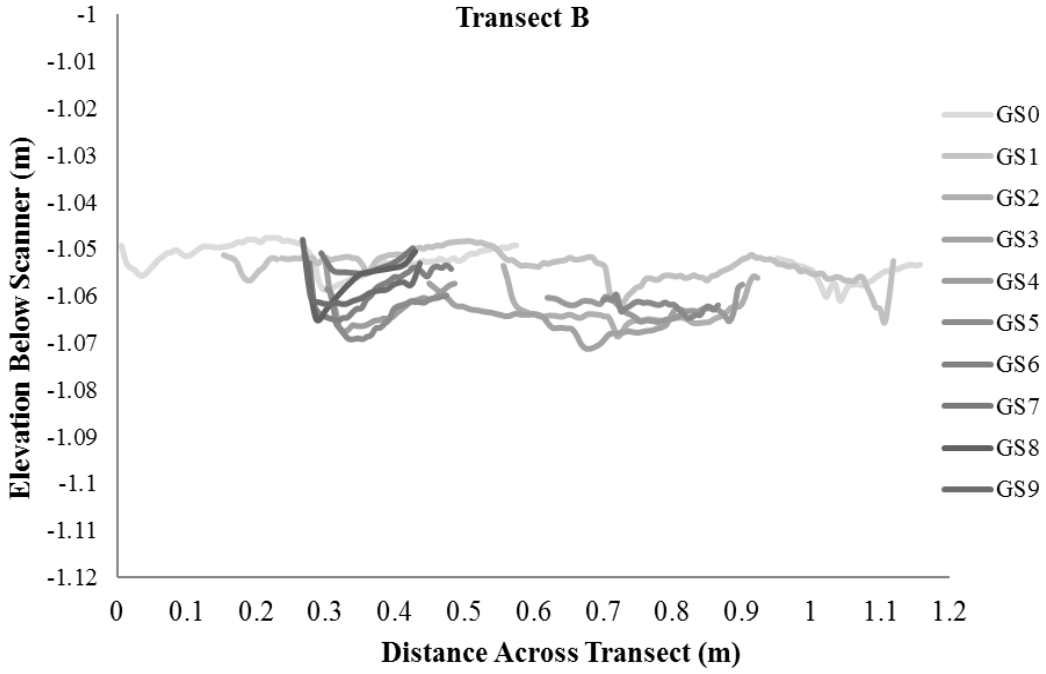

Figure 45. Experiment 2, Transect B elevation profiles.

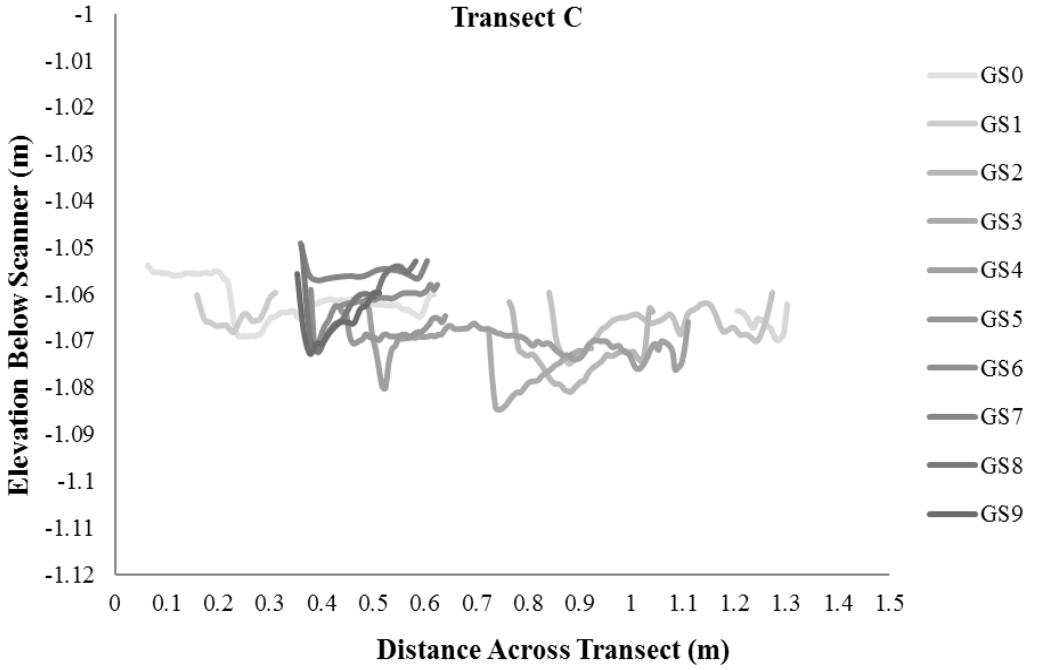

Figure 46. Experiment 2, Transect C elevation profiles.

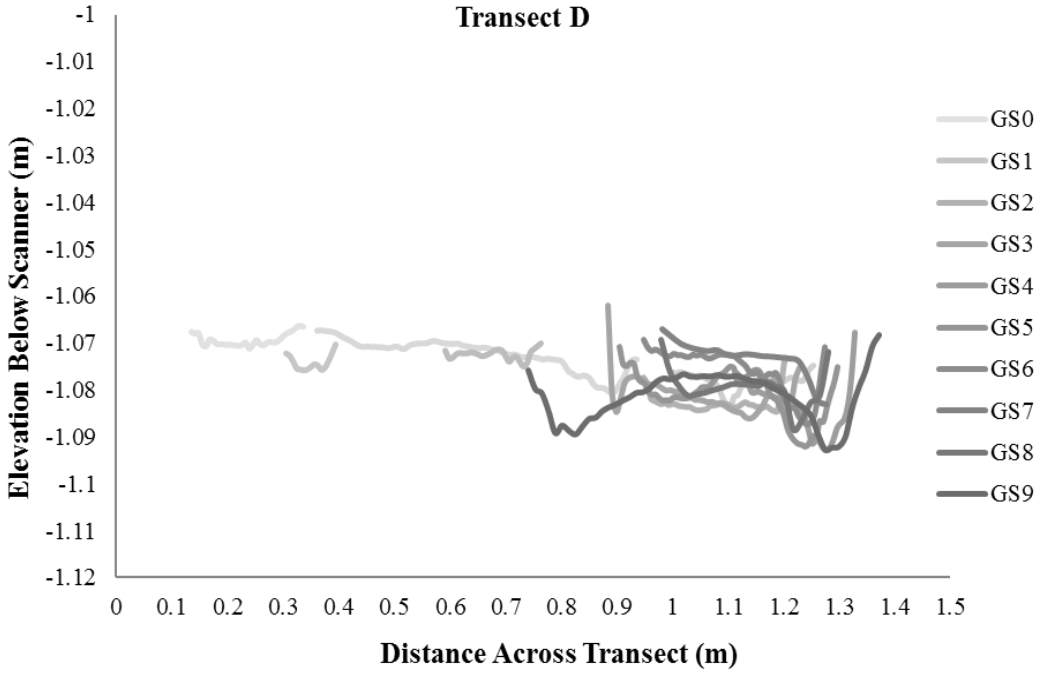

Figure 47. Experiment 2, Transect D elevation profiles.

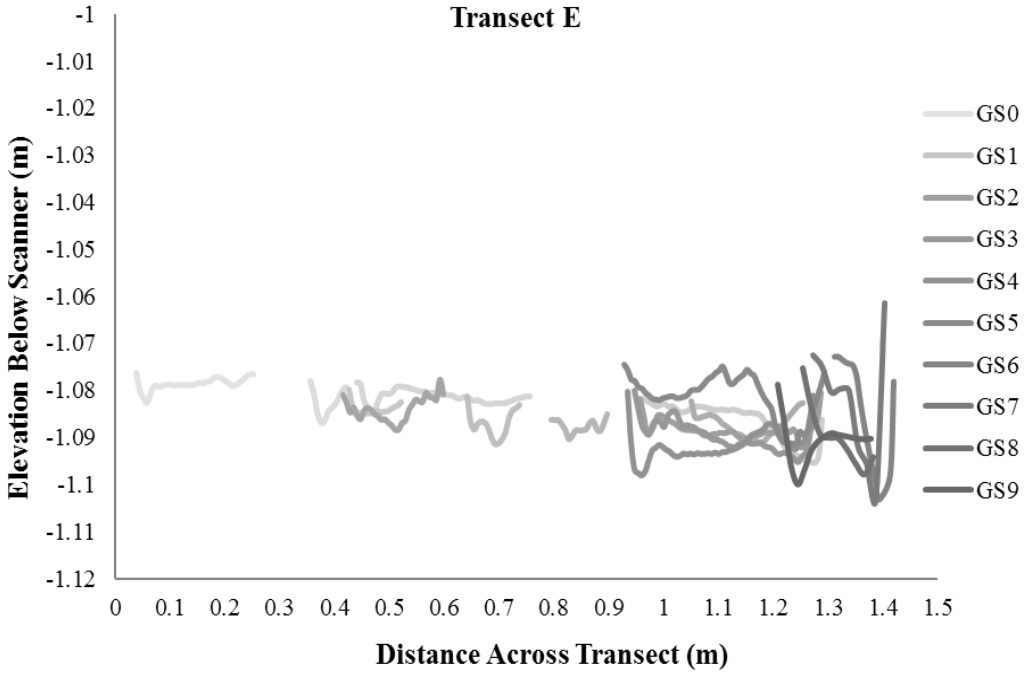

Figure 48. Experiment 2, Transect E elevation profiles.

Transect	GS0	GS1	GS2	GS3	GS4	GS5	GS6	GS7	GS8	GS9
A	147.5	130.0	92.0	82.0	58.3	36.3	24.4	25.0	25.0	34.3
B	260.0	146.7	61.7	61.7	94.0	21.3	18.2	16.3	17.8	18.9
C	162.0	98.3	46.7	15.4	62.0	36.3	30.0	40.0	22.9	26.7
D	257.5	120.0	37.1	42.5	44.0	10.0	10.8	11.1	8.3	8.3
E	232.5	108.0	85.0	55.0	51.7	74.0	55.0	8.7	10.0	21.3

Table 5. Experiment 2 width to depth ratios.

Fine Sediment Deposition and Floodplain Construction

A color threshold was applied to the high-resolution photographs taken from Camera 2 in order to highlight areas of sediment deposition during Experiment 2. These allowed us to observe changes in the spatial distribution of fine sediment. There was temporary fine sediment deposition on bars and low-flow channels in the absence of vegetation (GS0, Figure 50), though these deposits generally did not outlast the 4-hour

floods due to rapid reworking of the braidplain. During stages of low-density vegetation, (GS1-GS3, Figures 51-53), fines collected in low-flow channels, which were subsequently vegetated. As vegetation coverage and density increased, flow consolidated into fewer channels (GS4 and GS5, Figures 54 and 55), which eroded vegetated banks and developed alternating bars. Bars, both vegetated and unvegetated, collected fines particularly on headward and leeward ends. Over time, the channel bed began to rise, leading to bed aggradation and the reconnection of the channel with the floodplain. Fine sediment deposits were observed within the floodplain and in floodplain channels that were re-occupied by overbank flow (GS6 and GS7, Figures 56 and 57). In the final stages of the experiment, overbank deposition of fine sediment filled in chute cutoffs and other floodplain depressions (GS8 and GS9, Figures 58 and 59).

Figures 60-64 show manual transects measured across the entirety of all five transects at the end of GS2-GS8, including both floodplain and channel. Because floodplain surfaces could not be 'seen' by the lidar scanner, these transects provided the only estimate of changes in floodplain topography. Transects C, D, and E all demonstrate filling of floodplain channels after overbank flow started during GS6. Under overbank flow conditions, fine sediment was transported deep within the floodplain, collecting in depressions left by former low-flow channels that had been covered by vegetation. This led to an evening of the floodplain surface over time.

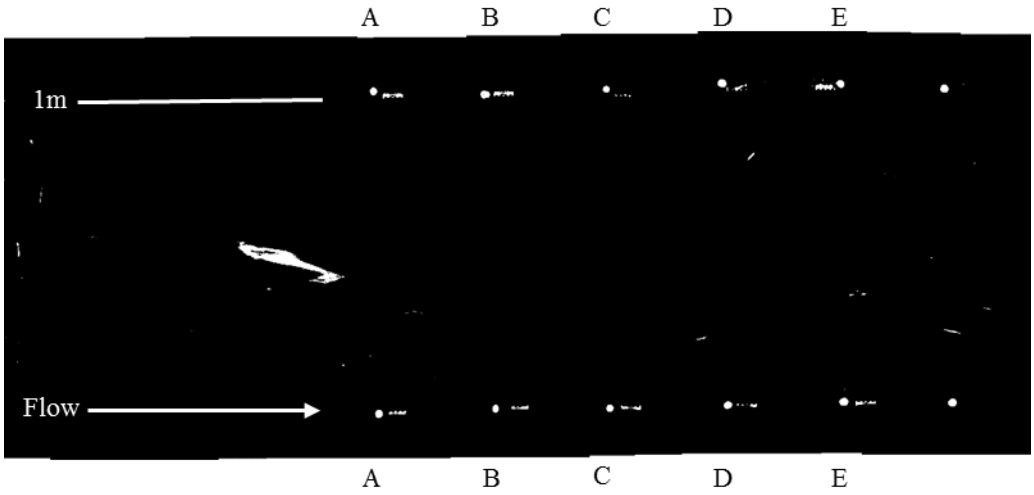

Figure 49. Experiment 2 fine sediment deposition after GS0.

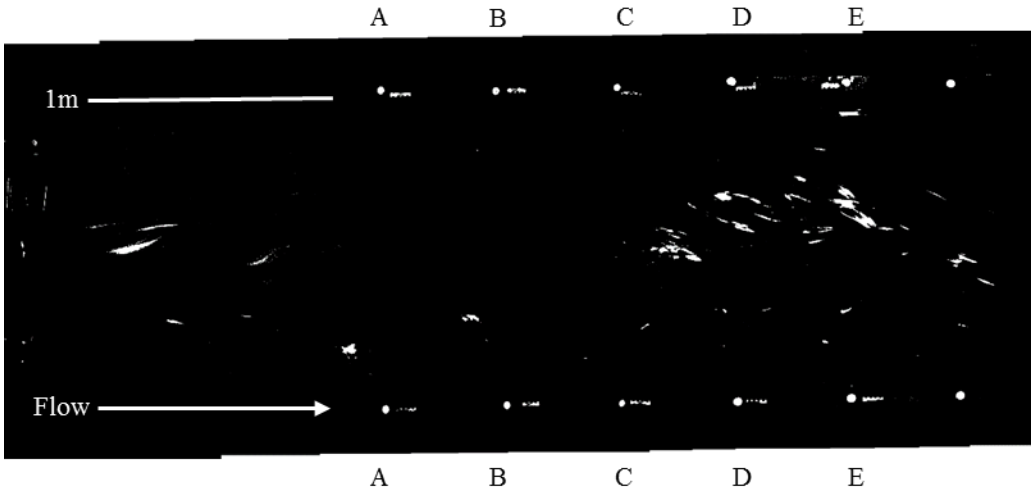

Figure 50. Experiment 2 fine sediment deposition after GS1.

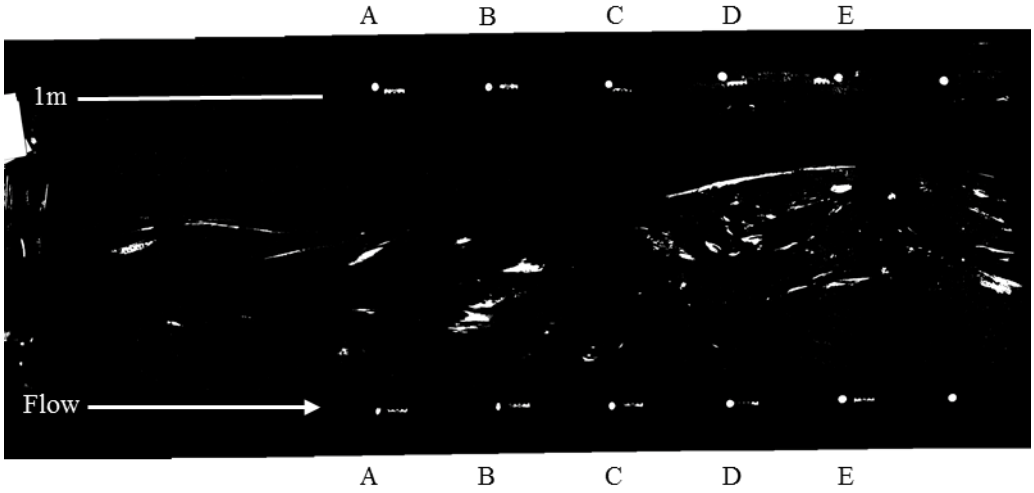

Figure 51. Experiment 2 fine sediment deposition after GS2.

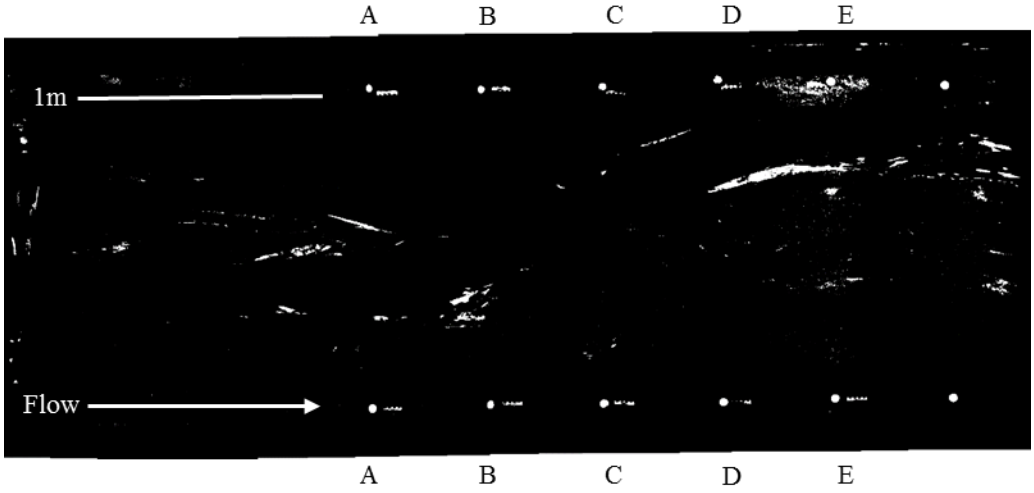

Figure 52. Experiment 2 fine sediment deposition after GS3.

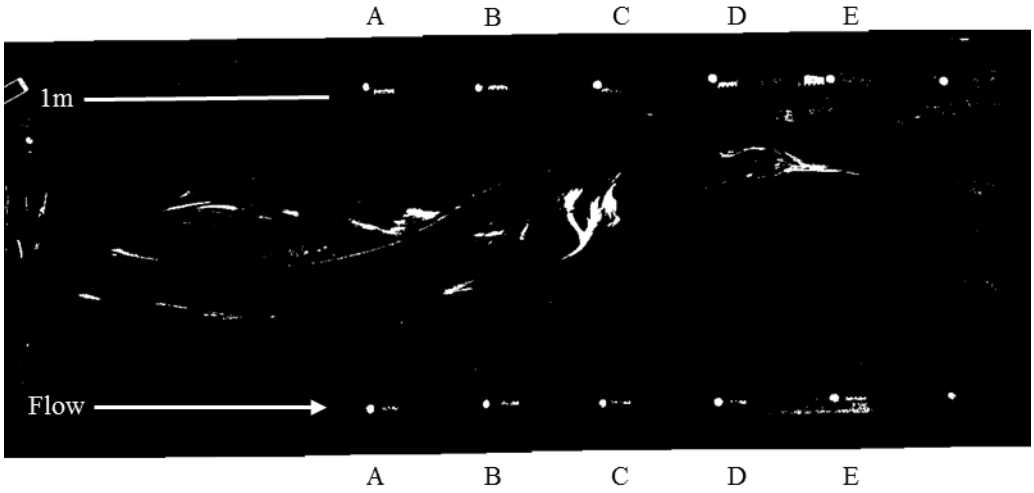

Figure 53. Experiment 2 fine sediment deposition after GS4.

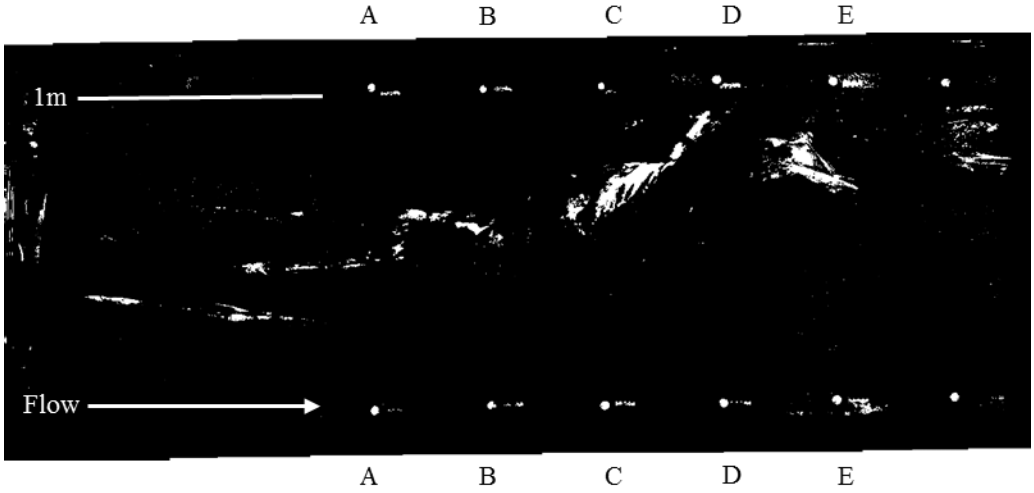

Figure 54. Experiment 2 fine sediment deposition after GS5.

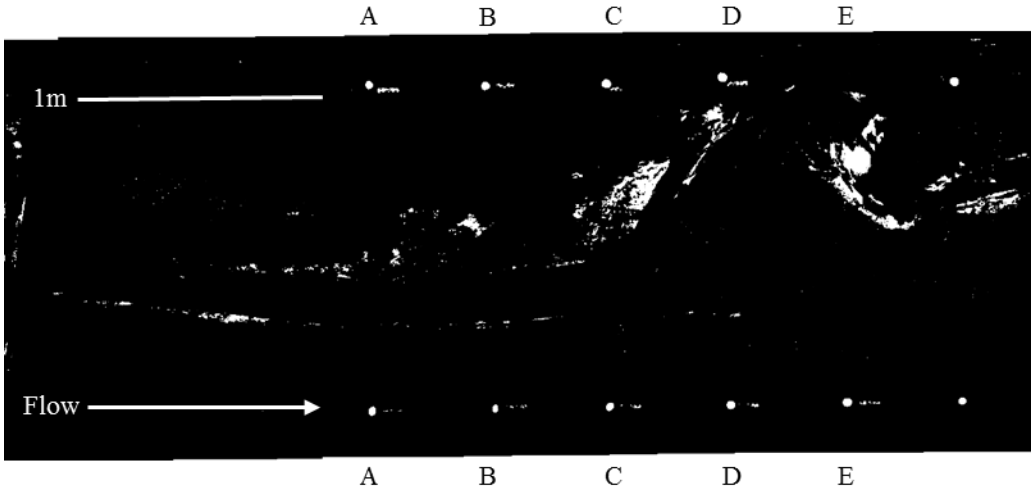

Figure 55. Experiment 2 fine sediment deposition after GS6.

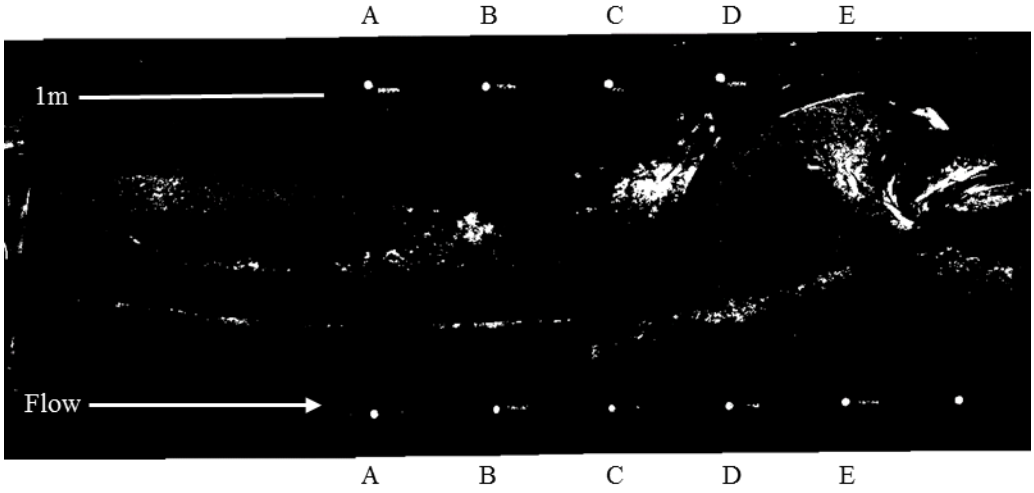

Figure 56. Experiment 2 fine sediment deposition after GS7.

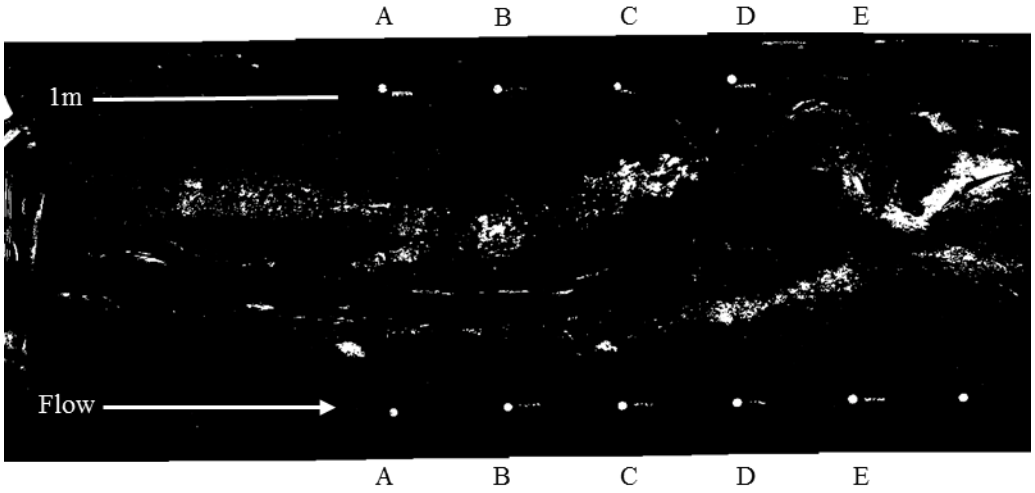

Figure 57. Experiment 2 fine sediment deposition after GS8.

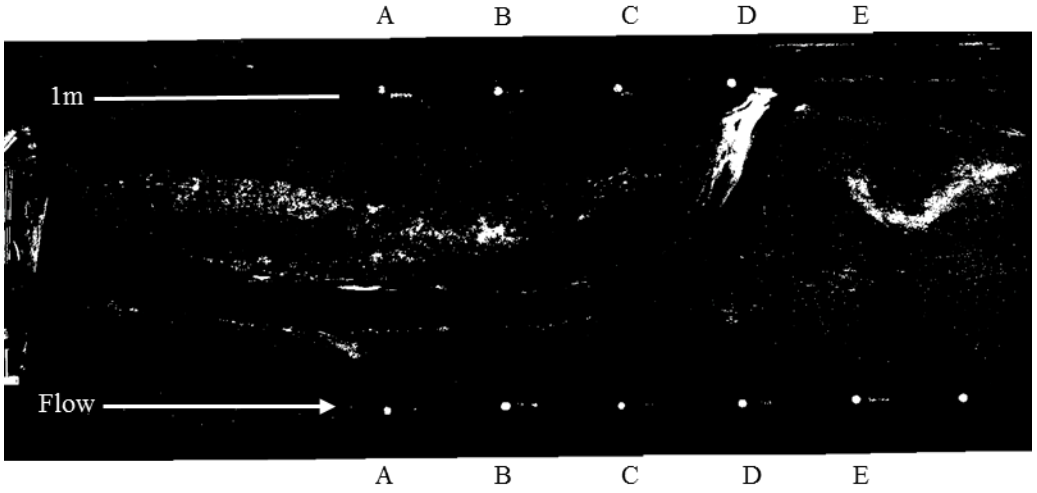

Figure 58. Experiment 2 fine sediment deposition after GS9.

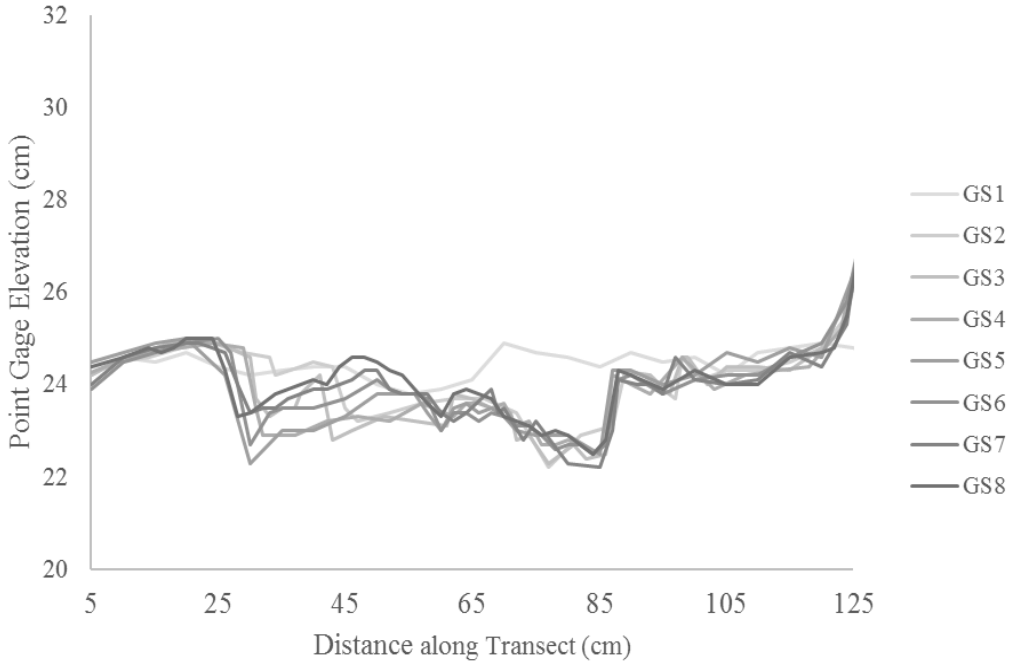

Figure 59. Experiment 2, Transect A floodplain elevation profiles.

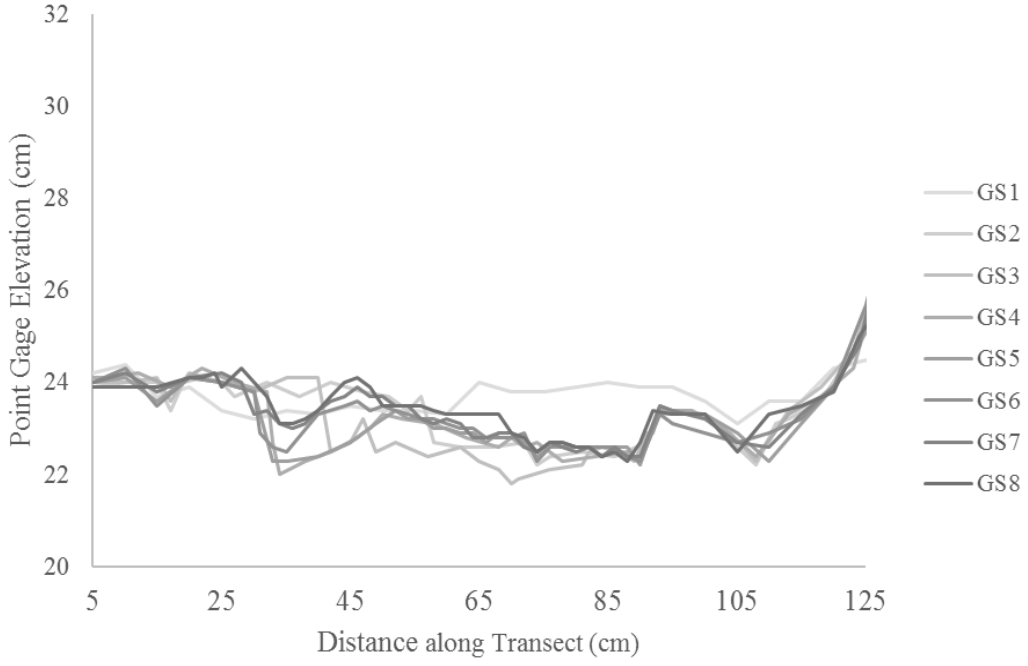

Figure 60. Experiment 2, Transect B floodplain elevation profiles.

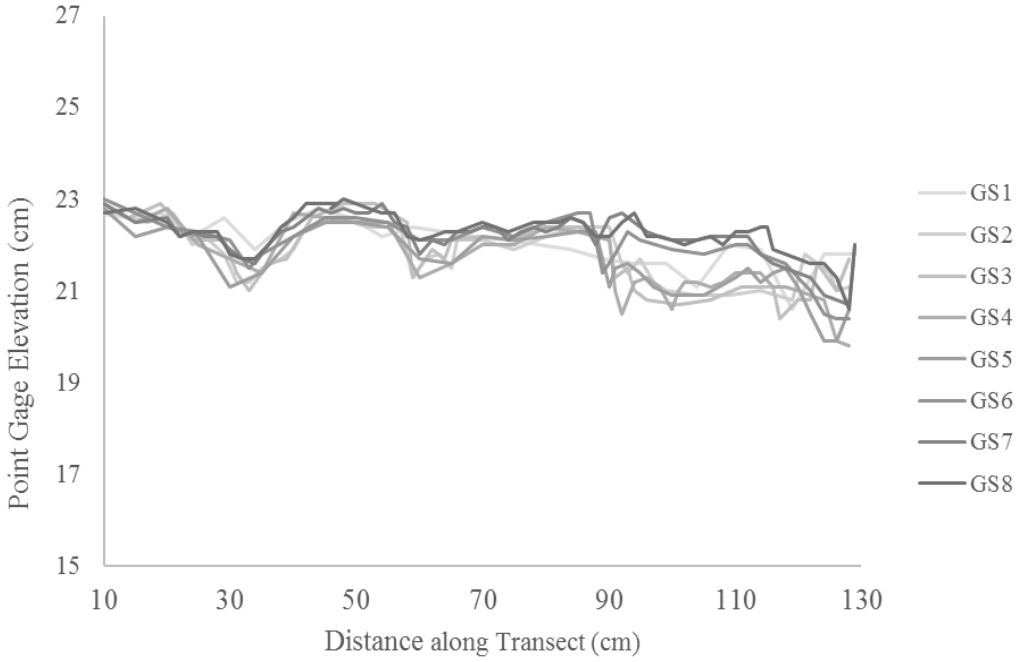

Figure 61. Experiment 2, Transect C floodplain elevation profiles.

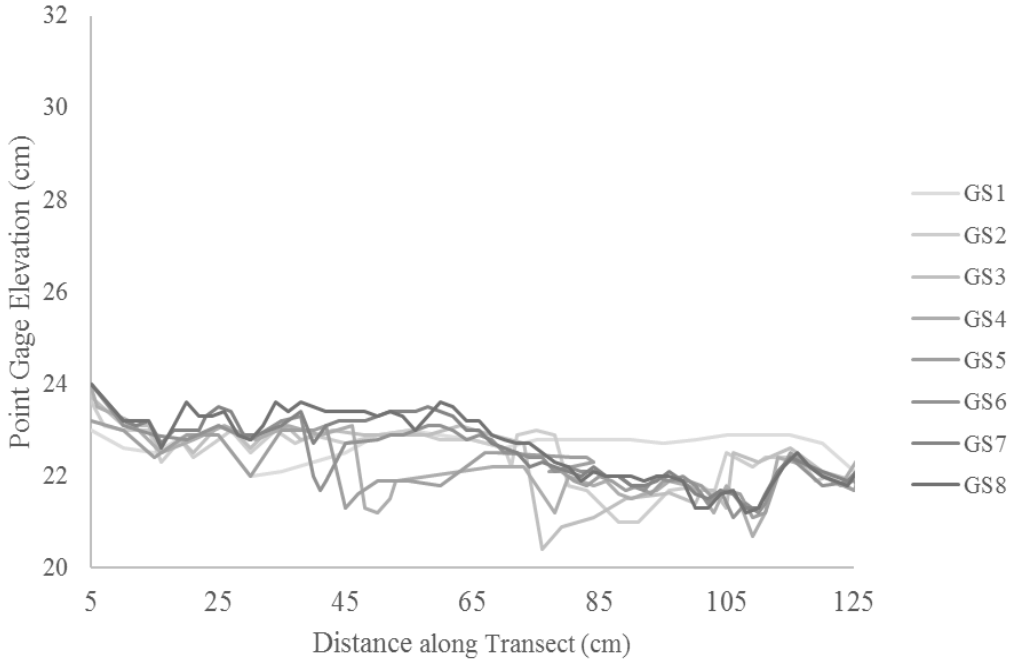

Figure 62. Experiment 2, Transect D floodplain elevation profiles.

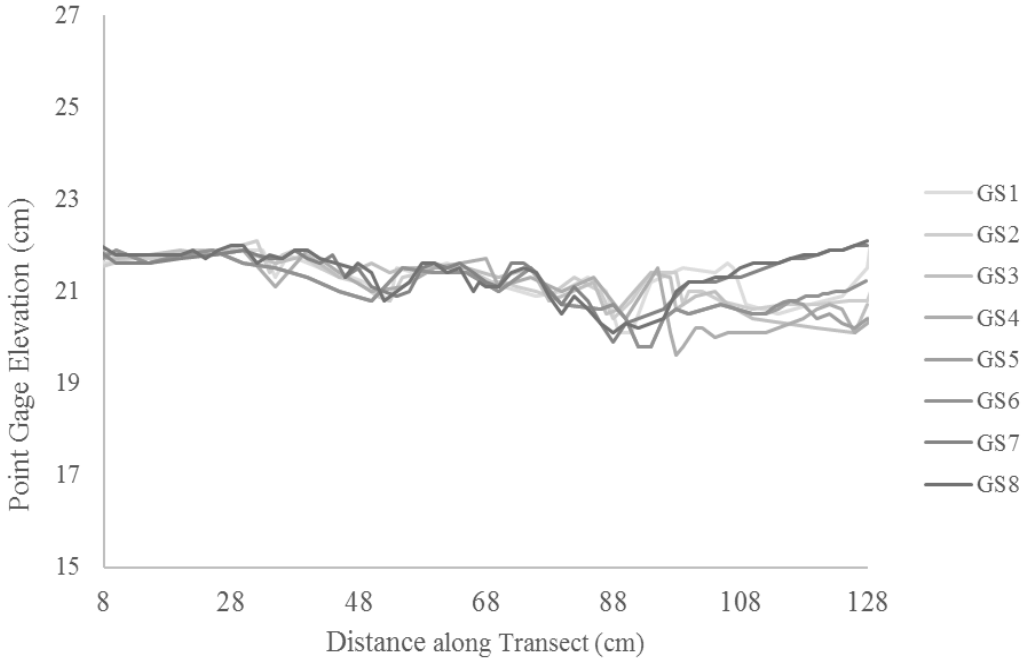

Figure 63. Experiment 2, Transect E floodplain elevation profiles.

Note: the active channel during GS6-8 had eroded the vegetated buffers along the sides of the flume, and flowed against the lateral wall. This was out of the reach of the point gauge; so, the active channel extends beyond 128 cm along Transect E during GS6-8.

Discussion

Experiment Comparison

In both experiments, the introduction of vegetation yielded a similar response to previous studies. Increased vegetation density and coverage forced narrower, deeper, and faster channels. However, varying sediment feed composition resulted in vastly different results between the two experiments in overall channel behavior as vegetation density increased with each flood. The composition of the sediment feed in Experiment 1 was 100% sand – the same composition as the flume bed – while the sediment feed used in

Experiment 2 contained 50% fine sediment by volume. The sediment feed rate was held constant at 1.3 g/s in both experiments.

Aggradation occurred to some degree in both experiments, starting within the upper 2m of the flume and continuing downstream. Conceptually, this makes sense. A constant sediment discharge forced into a channel increasingly constrained by vegetation, and therefore increasingly limited in lateral mobility, is likely to result in channel aggradation. In Experiment 1, channel elevation began to rise as early as GS2 and continued without interruption until the end of the experiment. I observed lobes of sand encroaching into the vegetated floodplain, particularly between Transects A-C. Sand could not be transported deep within the floodplain because of the presence of vegetation. Instead, it accumulated along the channel edge, generating levees and burying vegetation along the banks. Flow was forced around the raised channels and into the floodplain. Floodplain flows re-joined the main channel downstream, which had narrowed and deepened in response to a loss of available bed material trapped upstream. Rapid aggradation caused longitudinal variability in channel width, depth, velocity, and geometry in Experiment 1.

In Experiment 2, channel aggradation was not observed until GS6, after two avulsions during GS4 and GS5 had reduced the main channel to a single thread. The delay in channel aggradation allowed us to observe the expansion of meander bends through the pairing of inner bar deposition and outer bank erosion. Inner bars accumulated bed material during flood events. During 6-day inter-flood periods, vegetation grew on these newly formed point bars and enhanced bank strength, which

encouraged additional sand deposition and erosion of the outer bank during the next flood – a behavior characteristic of meandering rivers. This was not observed in Experiment 1 because rapid aggradation in the upper 3m of the flume forced channel flow into the floodplain, limiting the lateral mobility of the active channels. As a result, the main channel in Experiment 1 was very straight. In Experiment 2, eventual channel aggradation during GS6 induced overbank flow, which resulted in the re-occupation of previous low-flow channels. Fine sediment was transported deep within the floodplain, filling in these channels and contributing to floodplain construction. Aggradation during Experiment 2 only occurred between GS6-GS8, after which a channel cutoff around Transect D caused the channel to shorten and incise during GS9.

Channel-floodplain interactions were the main drivers of morphological differences between the two experiments. These interactions were initiated by aggradation, the timing and extent of which varied greatly between the two experiments due to varied composition of the sediment feed. The following discussion is a description and comparison of the respective roles of vegetation and sediment dynamics in the resulting channel-floodplain interactions and overall morphologic behavior.

The Role of Vegetation

Confirming the findings of other physical experiments as well as field observations, these experiments demonstrated that vegetation is not a passive but a dynamic component of fluvial systems. Vegetation played an active role in transitioning the physical characteristics of the system from an unstable, multi-threaded channel in a non-cohesive braidplain to a single-thread channel with a stable width and relatively low

rate of lateral migration within a well-defined floodplain. Vegetation also played an active role in the resulting morphological characteristics of each experiment by interacting with sediment load during conditions of overbank flow.

After the first seeding, low-density vegetation established in isolated 'patches', often referred to as 'pioneer landforms' (Gurnell et al., 2012). During the 6-day growth period between floods, the seeds germinated and sunk roots into the sand bed and in doing so enhanced surface cohesion in certain areas. During the subsequent flood, sprouts that were unable to take hold were eroded away, particularly during the first few floods. However, the rate of vegetation establishment remained greater than the rate of vegetation destruction during each flood, so vegetation coverage continued to increase. This positive feedback process is referred to as the 'ratchet effect' (Graf, 1978; Johnson, 1994; Tal et al., 2004; Corenblit et al., 2009). The progressive control of vegetation on channel mobility has been observed in the field (Graf, 1978; Gran et al, 2015) and replicated in the lab (Gran and Paola 2001, Tal et al, 2004; Tal, 2008). Our experiments were no exception, and the impacts of increased surface cohesion were the following:

1. Transition from "sweeping" laterally across the braidplain (unvegetated channel) to avulsing among fewer and fewer available pathways until only one remained.
2. Development of a well-defined floodplain that, once channel aggradation induced overbank flow, interacted with sediment load that ultimately led to the filling-in of floodplain depressions in Experiment 2.

3. Narrower, deeper and faster channels that were capable of eroding densely-vegetated outer banks and promoting the growth of inner bars.

Vegetation encroachment was responsible for the changes I observed in the distribution and mobility of bed load and suspended load. The expansion of vegetation coverage progressively limited the total area available for channel re-working and bedload deposition. This ultimately caused channel aggradation and forced overbank flow. In Experiment 1, early and rapid aggradation ultimately forced the channel to avulse into the floodplain. Floodplain vegetation barred sediment transport deep within the floodplain, causing levees to develop along the channel margin, extending downstream from the headwall between Transects A and C. This also starved downstream areas of bed material, which lead to channel incision and scour. Where aggradation was greatest, however, vegetation was buried and could not re-establish because any newly-deposited sprouts were also soon buried in sand. Gran et al. (2015) observed that vegetation was unable to establish on an aggrading braided river draining Mt. Pinatubo, a volcano in the Philippines. High sediment loads following a 1991 eruption caused higher lateral migration rates, which meant that the entire floodplain was reworked at a rate higher than that of vegetation establishment. Only when sediment load declined and aggradation slowed did lateral mobility decrease enough to allow vegetation to establish and persist within the floodplain.

The Role of Sediment

The differences in the timing and extent of channel aggradation are likely twofold. First, the feed rate of bed load was 50% greater in Experiment 1 than in Experiment 2. Second, the fine sediment fraction included in Experiment 2 was transported and deposited deep within the floodplain during overbank flow, filling in former channels and promoting floodplain construction. Which of these factors was more significant in determining the resulting channel patterns is difficult to determine based on the scope of information gathered and the limited number of experiments. However, the results from each of these experiments demonstrate that both coarse and fine sediment fractions played important roles in the resulting channel morphology. These differences became most evident once the channel had been reduced to a single thread and local aggradation forced overbank flow conditions.

Bed Load

In both experiments, bed load (sand) was critical in developing pioneer landforms – new surfaces upon which vegetation could germinate and sink roots (Gurnell et al., 2012). In the first few stages of both experiments, isolated patches of vegetation tended to expand and become both denser and stronger through time. Eventually, through the deposition of sand around them, these islands merged and formed the floodplain. The transport and deposition of sand as bed material made these landforms stable enough to support vegetation establishment.

Inner bars were also built by the deposition of sand that had been fed into the flume at the entrance or eroded from banks upstream. These bars became vegetated

through time, thus progressively strengthening inner bars, entrapping fine sediment and promoting outward meander migration.

Suspended Load

Braudrick et al. (2009) were among the first to use fine plastic sediment to simulate suspended sediment in experiments of this scale. They began with a single, straight channel in a bed of sand, and carved an initial bend near the inlet to initiate meandering. The experiment resulted in sustained meandering, where bank erosion and bar deposition rates, and therefore channel geometry remained stable. By filling in the upstream entrance of chutes that developed behind bars, fine sediment was critical in preventing meander cutoffs and allowing continued expansion of meander bends. In this way, fine sediment acted to seal the connection between bar and floodplain. While cutoffs did occur, in-filling of sediment slowed the rate of cutoffs and helped maintain channel width by balancing rates of bar growth and bank erosion. Though our flume was much smaller, I was able to observe similar patterns of bar deposition as well as the filling in of a single chute channel.

Our experiments began with a self-formed braided channel – unlike the experiment described by Braudrick et al., I had no influence on channel form once the initial straight channel disappeared entirely. Rather than focusing on generating self-sustaining meanders, our focus was on observing changes in vegetation-sediment interactions as vegetation density increased. In the absence of vegetation, fine sediment deposits were unable to withstand high lateral migration rates as the braided channel re-worked the entire width of the flume. When vegetation density was very low (GS1-2) and

channels were actively consolidating, incising and narrowing, I noticed some sediment deposition along the channel margins. These deposits were generally temporary, however, eroding away as channels adjusted laterally. By GS4, fewer, stronger channels began to erode into the vegetated banks, developing meander bends and two distinct point bars. Fine sediment began to accumulate on the upstream and downstream ends of these unvegetated point bars, however I posit that enhanced bank strength and additional bed load transport were primary drivers of channel movement during this period and that fine sediment played a more passive role in channel change or floodplain development. This changed in the second half of GS6 when channel aggradation forced channel flow over the banks, reconnecting the channel with the floodplain. At this point I began to observe fine sediment filling in former low-flow channels, smoothing out the topography of the floodplain. Channel-floodplain interaction through overbank flow was a critical pivoting point in terms of vegetation-fine sediment interactions. This marked the transition from fine sediment temporarily collecting along the channel margin and on channel bars, to permanent fine sediment deposits accumulating within the floodplain and actively contributing to floodplain construction. Results from both experiments demonstrated that more fine sediment was trapped within the vegetated floodplain once overbank flow conditions began.

While fine sediment deposition raised floodplain elevation and smoothed the topography, it is unlikely that this sediment contributed to enhanced surface strength. In natural rivers, I might expect the overbank deposition of cohesive fines (silt and clay) to further contribute to bank strength by adding surface cohesion. The plastic sediment used

here was non-cohesive, and once exposed to channel flow, was easily eroded. The primary roles of fine sediment in Experiment 2 were 1) filling in chutes that might otherwise lead to channel cutoffs, and 2) contributing to floodplain construction. The second was only made possible by the initiation of overbank flow, caused by progressive strengthening of the floodplain by vegetation.

Floodplain Development and Channel-Floodplain Connectivity

Floodplain connectivity, or the frequency and magnitude of channel-floodplain interactions, appears to have influenced how sediment was distributed and stored in each experiment. Overbank flow conditions, promoted by channel aggradation, allowed for sediment to be deposited and stored within the floodplain. What is the significance of floodplain sediment storage in natural river systems, and what significance might it have on a river's overall sediment budget? Vegetated floodplains can be complex elements in sediment transport systems, making their role in the sediment budget difficult to quantify. A study of two UK rivers, River Ouse and one of its tributaries, the River Wharfe (Walling et al., 1998) estimated using isotope measurements of sediment cores that floodplain storage represented 39% and 49% of each river's overall sediment budget, respectively. Storage in the channel beds of both rivers represented only 10% and 9%. However, the significance of floodplain storage will vary between rivers that differ in the amount of sediment being transported and the frequency of overbank flows (Wilkinson et al., 2014). Further, floodplain stores of fine sediment may eventually become sediment *sources* to rivers as channels rework the riparian corridor. Stout et al. (2014) estimated that fine sediment stored on the floodplain contributed up to 40% of the sediment input

into the Root River of southeastern Minnesota, though land use, basin size, and geomorphic setting influenced whether the majority of sediment load came from upland or near-channel sources.

Perhaps the most revealing way to understand the role that vegetated floodplains play in the transport and storage of sediment in rivers is to examine what happens when they are removed from the equation. What happens when natural or anthropogenic processes decrease the frequency and magnitude of channel-floodplain interactions, thus 'disconnecting' a channel from its floodplain? Channel-floodplain disconnection is part of the recent histories of many rivers in the United States. To enhance navigability and control flooding, major river channels are now flanked by levees that prevent overbank flows. The Mississippi River, for example, has over 2,200 miles of levees and is overall 150 miles shorter than it was in 1929 due to artificial shortening of its channel (Alexander et al., 2012). Other smaller streams have been artificially straightened or their sediment supplies limited, which tends to shorten river length and lead to incision (Shields et al., 1994). We noticed a similar effect towards the end of Experiment 2 when a cutoff occurred and the channel avulsed towards the lateral wall, which was followed by channel incision. Incision reduces the likelihood of overbank flow conditions because an incised channel can accommodate higher flows.

In summary, increasing vegetation density in both experiments resulted in the development of a vegetated floodplain which, once overbank flow conditions began, trapped and stored sediment more sediment than the unvegetated or sparsely-vegetated stages of each experiment. A channel's relationship with its vegetated floodplain,

determined by the frequency and magnitude of overbank flows, influences a river's ability to store sediment and therefore the floodplain's ability to evolve over time.

Conclusions

Our objective was to build upon previous flume experiments to observe vegetation-sediment interactions as vegetation density increases in a self-formed, coarse-bedded experimental river. These were generated through a series of floods followed by additional seeding of the flume surface. The only differences between the two experiments were the presence of a fine sediment fraction and the amount of bed load moving through the system, yet the resulting channel flow dynamics and planform characteristics were drastically different. High-magnitude floods combined with eventual channel aggradation caused by channel constriction by vegetation-induced overbank flow conditions, which in latter stages of our experiments connected the channel with the vegetated floodplain and forced vegetation-sediment interactions. The results highlight the following critical roles of riparian vegetation in the evolution of fluvial landforms:

1. Vegetation interacts with channel flow by adding turbulence and hydraulic drag, which can induce sediment deposition.
2. Vegetation constrains banks and controls lateral mobility of channels, which, during high-magnitude events lead to overbank flows, connecting the channel with its floodplain.
3. Vegetation adds surface cohesion and roughness to channel banks and the floodplain, which allow for the entrapment of sediment deposits. Coarse sediment deposits are crucial for developing new surfaces and connecting 'pioneer'

landforms to generate a floodplain. Coarse sediment cannot be carried through the floodplain and, when channel aggradation forces an avulsion, accumulates in levees along the channel margin. Fine sediment deposits accumulate first in topographic lows within the floodplain and over time act to raise the floodplain surface. Fine sediment also fills chute cutoffs, which has been demonstrated to deter head-cuts and promote meandering.

While it was clear through observations, time-lapse footage and photographs that vegetation combined with overbank flows allowed for fine sediment deposition deep within the floodplain, I did not quantify deposition or entrapment efficiency of vegetation through time. One way to do this would be to install a sediment trap at the end of the flume in order to measure sediment storage through time by mass balance. Repeat measurements would allow for the tracking of sediment trapping efficiency throughout different stages of the experiment. For example, I would have expected trapping efficiency to increase once overbank flow began in Experiment 2. In Experiment 1, I would have noticed a decrease in bed material leaving the flume once an aggradational fan developed in response to increased vegetation density.

Because of some logistical challenges, I was unable to achieve sustained, dynamic meandering in these experiments. First, this flume was rather short compared to those of similar studies, and the entrance effects (particularly a long and straight entrance channel) projected further down the length of the flume than anticipated. Second, once the channel eroded through the sand “buffers”, it tended to stick to the lateral walls. There was little I could do about this during the middle of an experiment, so I ended up with only one to

two meander bends during Experiment 2. However, the sediment deposits in former low-flow channels and chute channels are likely a critical component to sustained meandering. Similar studies of self-formed channels should be conducted on larger flumes to explore this further.

Bibliography

Alexander, J.S., R.C. Wilson, and W.R. Green, 2012, A brief history and summary of the effects of river engineering and dams on the Mississippi River system and delta. U.S. Geological Survey Circular 1375, 43 pp.

Beeson, C.E. and P.F. Doyle, 1995, Comparison of bank erosion at vegetated and non-vegetated channel bends. Journal of the American Water Resources Association, v. 31, n. 6, pp. 983-990.

Braudrick, C.A., W.E. Dietrich, G.T. Leverich, and L.G. Sklar, 2009, Experimental Evidence for the conditions necessary to sustain meandering in coarse-bedded rivers. Proceedings of the National Academy of Sciences of the United States of America, v. 106, n. 40, pp. 16936-16941.

Brooks, A.P., G.J. Brierley, and R.G. Millar. The long-term control of vegetation and woody debris on channel and flood-plain evolution: insights from a paired catchment study in southeastern Australia. Geomorphology, v. 51, pp. 7-29.

Chen, S., Y. Kuo, Y. Li, 2011, Flow characteristics within different configurations of submerged flexible vegetation. Journal of Hydrology, v. 398, pp.124-134.

Corenblit, D., E. Tabacchi, J. Steiger, and A.M. Gurnell, 2007, Reciprocal interactions and adjustments between fluvial landforms and vegetation dynamics in river corridors: A review of complimentary approaches. Earth Science Reviews, v. 84, pp. 56-86.

Erskine, W., A. Keene, R. Bush, M. Cheetham, and A. Chalmers, 2012, Influence of riparian vegetation on channel widening and subsequent contraction on a sand-bed stream since European settlement: Widden Brook, Australia. Geomorphology, v. 147-148, pp. 102-114.

Graf, W.L., 1978, Fluvial adjustment to the spread of tamarisk in the Colorado Plateau region. Geological Society of America Bulletin, v. 89, n. 10, pp. 1491-1501.

Gran, K. and C. Paola, 2001, Riparian vegetation controls on braided stream dynamics. Water Resources Research, v. 37 n. 12, pp. 3275-3283.

Gran, K.B, M. Tal and E.D. Wartman, 2015, Co-evolution of riparian vegetation and channel dynamics in an aggrading braided river system, Mount Pinatubo, Philippines. Earth Surface Processes and Landforms, v. 40, pp. 1101-1115.

Gurnell, A., W. Bertoldi, and D. Corenblit, 2012, Changing river channels: the roles of hydrological processes, plants and pioneer fluvial landforms in humid temperate, mixed load, gravel bed rivers. Earth Science Reviews, v. 111, pp. 129-141.

Gurnell, A., 2013, Plants as river systems engineers. Earth Surface Processes and Landforms, v. 39, pp. 4-25.

Gurnell, A.M., J.M. Goodson, P.G. Angold, I.P. Morrissey, G.E. Petts, and J. Steiger, 2004, Vegetation propagule dynamics and fluvial geomorphology. Water Science and Application 8: Riparian Vegetation and Fluvial Geomorphology, p. 209-219.

Hession, W.C., J.E. Pizzuto, T.E. Johnson, and R.J. Horwitz, 2003, Influence of bank vegetation on channel morphology in rural and urban watersheds. Geology, v. 31, pp. 147-150.

James, C.S., A. L. Birkhead, A. A. Jordanova and J. J. O'Sullivan, 2004, Flow resistance of emergent vegetation. Journal of Hydraulic Research, v. 42, n. 4, pp. 390-398.

Leopold, L. B. and M. G. Wolman 1957, River channel patterns: braided, meandering, and straight, vol. 282-B. Geological Survey Professional Paper.

Liu, D., P. Diplas, CC. Hodges and J.D. Fairbanks, 2010, Hydrodynamics of flow through double-layer rigid vegetation. Geomorphology, v.16, pp. 286-296.

Luhar, M. and H.M. Nepf, 2013, From the blade scale to the reach scale: a characterization of aquatic vegetative drag. Advances in Water Resources, v. 52, pp. 305-316.

Martin, J. M., and M. Meybeck, 1979, Elemental mass balance of material carried by major world rivers. Marine Chemistry, v. 7, pp. 173–206.

Millar, Robert G., 2000, Influence of bank vegetation on alluvial channel patterns. Water Resources Research, v. 36, n. 4, pp. 1109-1118.

Murray, A.B., M.A.F. Knaapen, M. Tal, and M.L. Kirwan, 2008, Biomorphodynamics: Physical-biological feedbacks that shape landscapes. Water Resources Research, v. 44, pp. 1-18.

Nepf, H.M., 1999, Drag, turbulence, and diffusion in flow through emergent vegetation. Water Resources Research, v. 35, 479–489.

Nepf, H.M., 2012, Hydrodynamics of vegetated channels. Journal of Hydraulic Research, v. 50, n. 3, pp. 262-279.

Nilsson, C., M. Gardfjell, and G. Gresslon, 1991, The importance of hydrochory in structuring plant communities along rivers. Canadian Journal of Botany, v. 69, n. 12, pp. 2631-2633.

O'Hare, M.T., C. McGahey, N. Bisset, C. Cailes, P. Henville, and P. Scarlett, 2010, Variability in roughness measurements for vegetated rivers near base flow, in England and Scotland. Journal of Hydrology, v. 385, pp. 361-370.

Operstein, V. and S. Frydman, 2000, The influence of vegetation on soil strength. Proceedings of the Institution of Civil Engineers – Ground Improvement, v. 4, n. 2, pp. 81-89.

Paola, C., 2001, Modelling stream braiding over a range of scales, in *Gravel Bed Rivers V*, Mosely MP (ed.). New Zealand Hydrological Society: Wellington, pp. 11-46.

Paola, C., K. Straub, D. Mohrig, and L. Reinhardt, 2009, The 'unreasonable effectiveness' of stratigraphic and geomorphic experiments, Earth Science Reviews, p. 97, pp. 1-43.

Rowntree, K.M. and E.S.J. Dollar, 1999, Vegetation controls on channel stability in the Bell River, Eastern Cape, South Africa. Earth Surface Processes and Landforms, v. 24, n. 2, pp. 127-134.

Shields, F.D., S.S. Knight, and C.M. Cooper, 1994, Effects of channel incision on base flow stream habitats and fishes. Environmental Management, v. 18, n. 1, pp. 43-57.

Sigafoos, R.S., 1961, Vegetation in relation to flood frequency near Washington, D.C., U. S.A. Geological Survey Professional Paper 424-C, pp. 248–249.

Stout, J.C., P. Belmont, S.P. Schottler and J.K. Willenbring, 2014, Identifying sediment sources and sinks in the Root River, southeastern Minnesota. Annals of the Association of American Geographers, v. 104, n. 1, pp. 20-39.

Tabacchi, E., L. Lambs,1 H. Guilloy, A. Planty-Tabacchi, E. Muller, and H. Décamps, 2000, Impacts of riparian vegetation on hydrological processes. Hydrological Processes, v. 14, n. 16-17, pp. 2959-2976.

Tal, M., K. Gran, A.B. Murray, C. Paola, and D. M. Hicks, 2004, Riparian vegetation as a primary control on channel characteristics in multi-thread rivers. Water Science and Application 8: Riparian Vegetation and Fluvial Geomorphology, S.J. Bennett and A. Simon (eds.), pp. 43-58.

Tal, M. and C. Paola, 2007, Dynamic single-thread channels maintained by the interaction of flow and vegetation. Geology, v. 35, pp. 347-350.

Tal, M. 2008. Interactions between vegetation and braiding leading to the formation of single-thread channels in a laboratory experiment, PhD Thesis. University of Minnesota, Minneapolis; 178.

Tal, M. and C. Paola, 2010, Effects of riparian vegetation on channel morphodynamics: results and insights from laboratory experiments. Earth Surface Processes and Landforms, v. 35, pp. 1014-1028.

van Dijk, W.M., W. I. van de Lageweg, and M. G. Kleinhans, 2012, Experimental meandering river with chute cutoffs, Journal of Geophysical Research, v. 117,

van Dijk, Wout M., 2013, Meandering rivers – feedbacks between channel dynamics, floodplain and vegetation (Doctoral dissertation). Accessed online from the Utrecht University Repository ISBN 978-90-6266-329-3.

Walling, D.E., P.N. Owens, and G.J.L. Leeks, 1998, The role of channel and floodplain storage in the suspended sediment budget of the River Ouse, Yorkshire, UK. Geomorphology, v. 22, pp. 225-242.

Wilkinson, S.N., C. Dougall, A.E. Kinsey-Henderson, R.D. Searle, R.J. Ellis and R. Bartley, 2014, Development of a time-stepping sediment budget model for assessing land-use impacts in large river basins. Science of the Total Environment, v. 468-469, pp. 1210-1224.

Faro Focus 3-D Laser Scanner. Tech Sheet. Web. <http://www.faro.com/focus/us/downloads>.

Appendix 1. Critical Depth for Sediment Mobility

We used the Shields parameter to determine the threshold depth for sediment mobility. The Shields parameter, τ^* is a dimensionless number that relates driving forces on a particle vs. the force of that particle's resistance:

$$\tau^* = \tau_b / (\rho_S - \rho)gD_{50}$$

Where g is the force of gravity (9.8 kg/m^2) ρ is the density of water (1000 kg/m^3) ρ_S is sediment density (2650 kg/m^3 for the quartz sand, 1250 kg/m^3 for the plastic sediment), and D_{50} is median grain size in m (0.005 m for quartz sand, 0.0015 m for the plastic sediment), and τ_b is the shear stress acting on the bed, determined by the depth-slope product:

$$\tau_b = \rho ghS$$

Where S is slope (0.015). All of the above variables are known except for h, which is depth in meters. The Shields diagram relates the Shields parameter with the particle Reynolds number, Re:

$$Re = u^*D_{50}/\nu$$

Where ν = kinematic viscosity ($1.5x10^{-6}$ m^2/s), and u^* is shear velocity:

$$u^* = (\tau_b/\rho)^{0.5}$$

The curve displayed on the Shields diagram is the threshold for mobility:

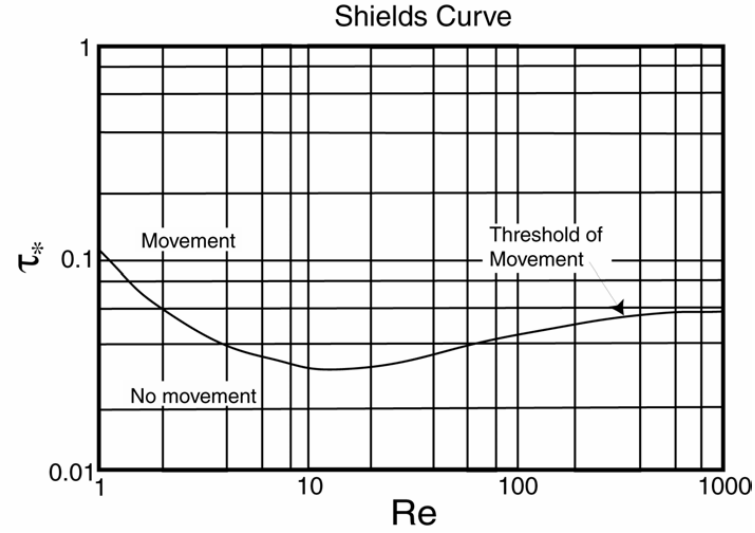

Using our parameters for the sand, if one applies an h value of 0.002 m for calculations of τ* and Re, the resulting τ* value of 0.036 and a Re value of 5.64. Plotted on the Shields diagram, this point lies directly on the Shields curve. Therefore, we determined that a particle of 0.5 mm quartz sand on the bed surface would be mobile in depths above 2 mm. Doing the same for the plastic sediment, I calculated that the sediment should be mobile at 0.8 mm (τ* = 0.32, Re = 1.07). The Rouse number (Appendix 2) would indicate at what depths the fine sediment fraction would be mobilized as bed load or as suspended load.

Calculation for Quartz Sand				
Parameter	Symbol	Unit	Formula	Value
density of sediment	ρ_S	kg/m^3	---	2650
density of water at 5°C	ρ	kg/m^3	---	1000
specific gravity of sediment	R	---	$R = (\rho_S-\rho)/\rho$	1.65
dynamic viscosity of water at 5°C	μ	$N\ s/m^2$	---	0.00152
kinematic viscosity	υ	m^2/s	$\upsilon = \mu/\rho$	1.52E-06
acceleration of gravity	g	m/s^2	---	9.81
von Karman constant	κ	---	---	0.41
particle diameter	D	m	---	0.0005
slope	S	---	---	0.015
critical depth	h	m	---	0.002
bed shear stress	τ_b	N/m^2	$\tau b = \rho ghS$	0.294
Shields parameter	τ^*	---	$\tau c^* = \tau b / [(\rho s-\rho)gD]$	0.036
shear velocity, u*	u*	---	$u^* = (\tau b/\rho)^{0.5}$	0.017
boundary particle Reynolds no.	Re	---	$Re_p^* = u^*D/\upsilon$	5.64

Calculation for Plastic Sediment (Clear Cut)				
Parameter	Symbol	Unit	Formula	Value
density of sediment	ρ_S	kg/m^3	---	1250
density of water at 5°C	ρ	kg/m^3	---	1000
specific gravity of sediment	R	---	$R = (\rho_S-\rho)/\rho$	0.25
dynamic viscosity of water at 5°C	μ	$N\ s/m^2$	---	0.00152
kinematic viscosity	υ	m^2/s	$\upsilon = \mu/\rho$	1.52E-06
acceleration of gravity	g	m/s^2	---	9.81
von Karman constant	κ	---	---	0.41
particle diameter	D	m	---	0.00015
slope	S	---	---	0.015
critical depth	h	m	---	0.0008
bed shear stress	τ_b	N/m^2	$\tau b = \rho ghS$	0.118
Shields parameter	τ^*	---	$\tau c^* = \tau b / [(\rho s-\rho)gD]$	0.320
shear velocity, u*	u*	---	$u^* = (\tau b/\rho)^{0.5}$	0.011
boundary particle Reynolds no.	Re	---	$Re_p^* = u^*D/\upsilon$	1.07

Appendix 2. The Rouse Number

To simulate suspended load, I used a non-cohesive plastic sediment with a median grain size of 0.15 mm and a specific gravity of 1.25. To ensure that this sediment behaves as suspended or partially suspended load, we can consider the Rouse number, P:

$$P = \frac{U}{ku*}$$

where k is the von Karman constant (0.41), u* is the shear velocity:

$$u* = (\tau_b/\rho)^{0.5}$$

where τ_b is shear stress acting on the bed (kg/m^2) determined by the depth-slope product,

$$\tau_b = \rho g h S$$

where g is the force of gravity ($9.8\ m/s^2$), ρ is the density of water ($1000\ kg/m^3$), and S is slope (0.015). U is the settling velocity in m/s as determined by the Turbulent Drag Law (for particles > 0.1 mm; Stokes law is used for particles < 0.1 mm):

$$U = [(0.66Dg(\rho_S-\rho))/\rho]^{0.5}$$

Plotting the Rouse number as a function of expected flow depths, below, we see that the synthetic sediment (D_{50} = 0.15mm, SG = 1.3) should behave as fully suspended load (100% of input in suspension) in depths greater than about 1 cm, and as partially suspended load (50% of input in suspension) at flow depths between 0.2-1 cm. It should be noted that these estimations do not consider roughness, provided by the bed or by vegetation on channel bars. Such roughness may induce deposition at depths where the sediment is thought to be in suspension. However, for our expected range of flow depths

– 0.2 – 4 cm, the plastic sediment should behave as partially suspended to fully suspended load.

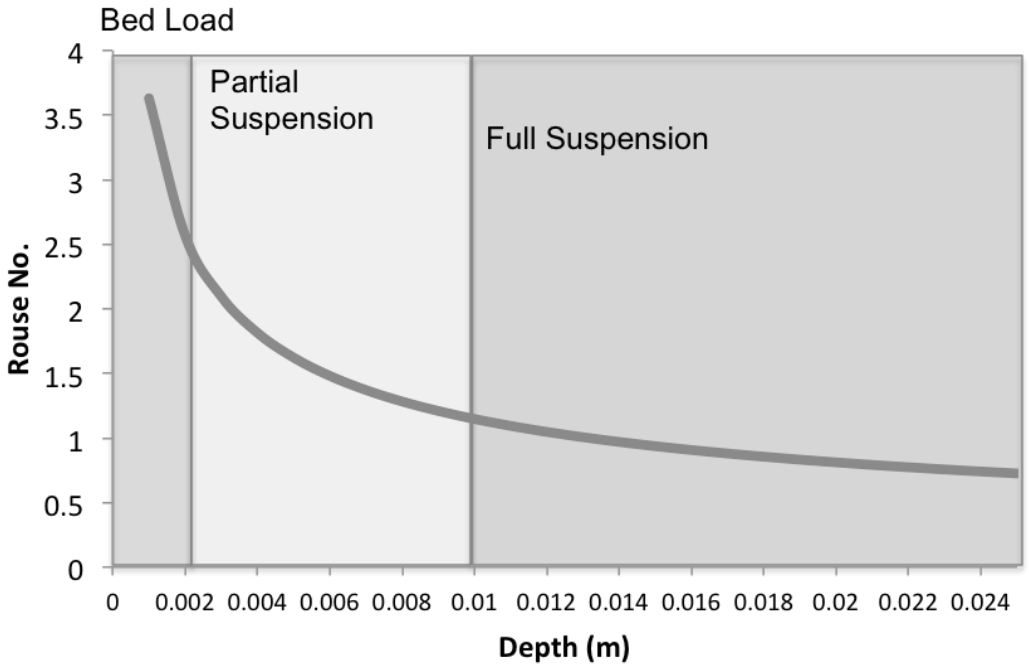

Rouse Number for the plastic sediment (D_{50} = 0.15 mm, ρ_S = 1.25) as a function of flow depth (h). Slope is 0.015. Rouse numbers greater than about 2.5 indicate bedload, 1.2-2.5 Indicates 50% suspension, 0.8-1.2 indicates 100% suspension, and < 0.8 indicates wash load.